Electrostatic Potentials in Rhodopseudomonas viridis Reaction Centers: Implications for the Driving Force and Directionality of Electron Transfer†

1 AUTHOR:

Marilyn R Gunner
City College of New York

72 PUBLICATIONS **4,352** CITATIONS

SEE PROFILE

Electrostatic Potentials in *Rhodopseudomonas viridis* Reaction Centers: Implications for the Driving Force and Directionality of Electron Transfer[†]

M. R. Gunner*

Department of Physics, City College of New York, 138th St. and Convent Avenue, New York, New York 10031

Anthony Nicholls and Barry Honig

Department of Biochemistry and Molecular Biophysics, Columbia University,
630 W. 168th St. New York, New York 10032

Received: July 6, 1995; In Final Form: October 19, 1995[⊗]

Finite difference solutions to the Poisson equation are used to characterize electrostatic interactions in reaction centers from *Rhodopseudomonas viridis*. A sizable potential gradient resulting primarily from charged amino acid side chains is found in the protein. This static field favors the observed electron transfers from the primary donor (P) along the L branch of the protein via the bacteriochlorophyll monomer (B_L) toward the bacteriopheophytin electron acceptor (H_L). The effect of the field is to favor electron transfer to B_L by approximately 0.4 eV and to H_L by approximately 0.8 eV. The electric field along the M branch is significantly smaller, thus providing a straightforward explanation for the directionality of electron transfer. The large static field in the protein appears to be necessary to overcome the intrinsic cost of charge separation in a low dielectric medium. Electrostatic potentials were calculated for the protein in uniform low dielectric medium and for the protein surrounded by water with and without a membrane. While the calculated site potentials are sensitive to the assumptions about the dielectric response of the protein and surrounding medium, the conclusion that there is a large static field favoring charge separation along the L branch is independent of the detailed model used to describe the system.

Introduction

Photosynthetic reaction centers (RC) are proteins that store a photon's energy via a series of electron-transfer reactions. RCs from *Rhodopseudomonas viridis* contain two bacteriochlorophylls which form a strongly coupled dimer known as the special pair (P), two accessory bacteriochlorophylls, B_L and B_M, two bacteriopheophytins, H_L and H_M, a menaquinone, Q_A, and ubiquinone, Q_B (see Figure 1). Electron transfer is initiated by the absorption of a photon by P generating an excited singlet state (P*). Within 3 ps an electron is transfered to H_L, located 18 Å away, forming $P^+H_L^-$. In 200 ps the electron is transferred to Q_A and then in 200 μs to Q_B Electron transfer proceeds along the L branch of the RC while the M branch is inactive. Except for the electron transfer from Q_A to Q_B, each of these electron-transfer reactions occurs with only small differences in rate from 1 K to room temperature (see references 1−3 for reviews).

The RC from the bacteria *Rps. viridis* was the first integral membrane protein to have a structure solved to atomic resolution.[4,5] Since then a higher resolution structure from *Rps. viridis*[6] and several structures from *Rhodobacter sphaeroides* have become available.[4,5,7−10] In this paper we use the methods of classical electrostatics to consider how the RC structure is designed to facilitate the rapid, unidirectional separation of charge even at cryogenic temperatures.

Three specific questions will be addressed here. The first concerns the free energy difference between P* and $P^+H_L^-$,

which has been measured to be approximately −250 meV.[11−13] First we consider how electron transfer to form an ion pair, which is generally an uphill reaction in low dielectric media, can be stabilized in the interior of a membrane protein. The second question concerns the role of the bacteriochlorophyll monomer, B_L, which lies between P and H_L. It seems inescapable that this group facilitates electron transfer from P to H_L. The observed rate of electron transfer from P to H_L of 5×10^{11}/s is consistent with two short tunneling steps but is 10^3 times faster than expected for a single 18 Å transfer.[14−16] However, the specific role of B_L is unclear. B_L can facilitate electron transfer either by a superexchange mechanism or as a direct intermediate which is transiently reduced.[17−24] The free energy of the $P^+B_L^-$ state relative to P*, which determines what role this state can play, is considered below. The third question concerns the inactive bacteriochlorophyll (B_M) and bacteriopheophytin (H_M) on the M branch which form a second possible pathway for charge separation. Despite the pseudo-symmetry of the RC structure, electron transfer proceeds via the L branch alone. The mechanism that determines the choice of pathway is also an open question.

Electron transfer in RCs has been the subject of numerous theoretical investigations which have focused primarily on the role of B_L and the M branch. Quantum mechanical calculations have been carried out of the electronic states of the cofactors.[25−30] Molecular dynamics simulations have explored the nuclear motions that accompany electron transfer.[31−40] Several estimates have been made of the contribution of the protein to the electrostatic potentials at the cofactors,[41,42] and electrostatic analysis has estimated the contribution of the protein to the free energy of charge separation.[39,40,43]

The work presented here uses finite difference solutions to the Poisson equation to calculate the electrostatic free energy of the various states. The primary finding is that the protein

---

[†] Abbreviations: P bacteriochlorophyll dimer. B_L active, L branch bacteriochlorophyll monomer. B_M inactive, M branch bacteriochlorophyll monomer. H_L active, L branch bacteriopheophytin. H_M inactive, M branch bacteriopheophytin. β_L a bacteriochlorophyll in the H_L site. PCW charges for ground state and ionized cofactors taken from ref 43. BChl bacteriochlorophyll. BPh bacteriopheophytin. Regions of different dielectric constants are denoted: ϵ_{prot}:ϵ_{solv}:ϵ_{mem} or ϵ_{prot}:ϵ_{solv}.
[⊗] Abstract published in *Advance ACS Abstracts,* January 1, 1996.
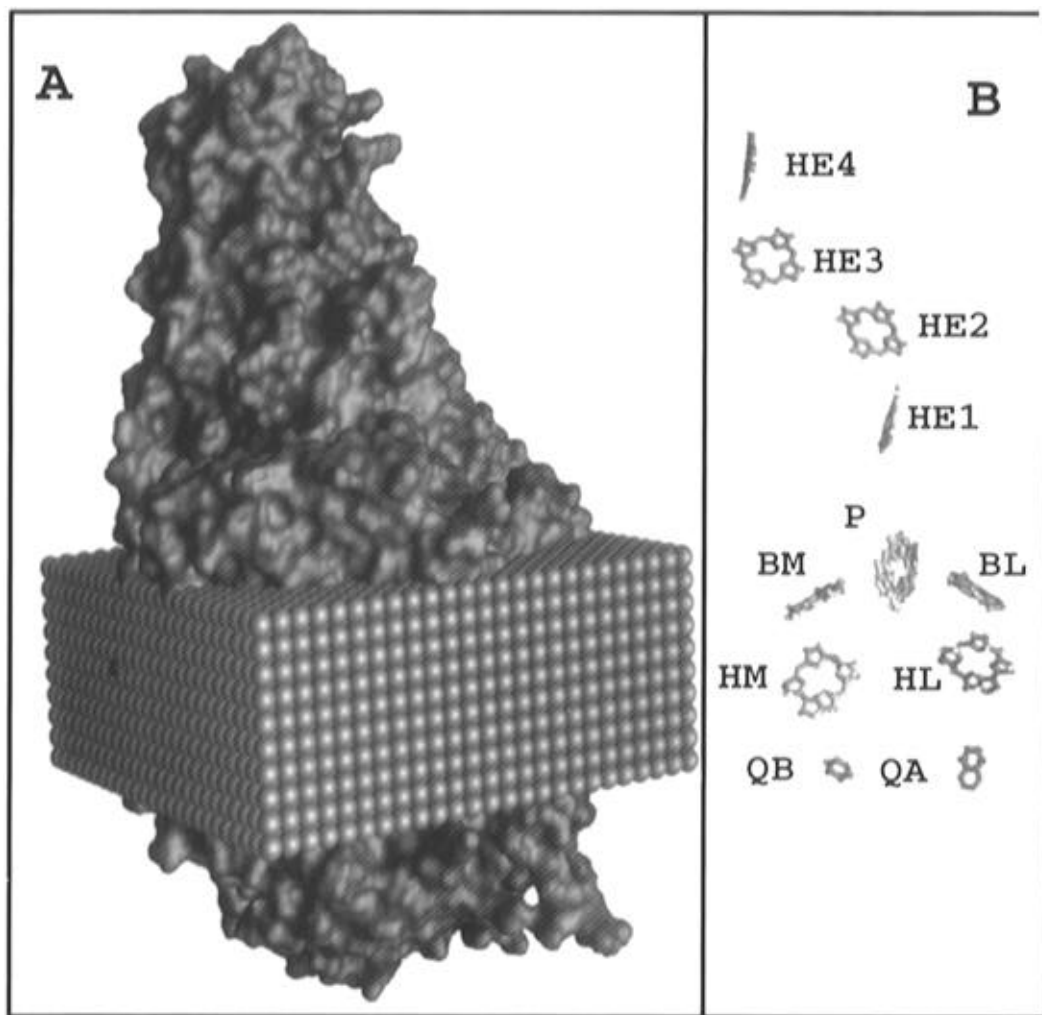
Figure 1. (A) Shape of the low dielectric region encompassed by the *Rps. viridis* RC and the model membrane. (B) The cofactors: P bacteriochlorophyll dimer which is the electron donor; B_L is the active, L branch bacteriochlorophyll monomer; B_M the inactive, M branch bacteriochlorophyll monomer; H_L is the active, L branch bacteriopheophytin; H_M is the inactive, M branch bacteriopheophytin. He1−He4 are the four hemes in the cytochrome subunit.

sets up a strong static field resulting from charged and polar groups that stabilizes the charge transfer states $P^+B_L^-$ and $P^+H_L^-$ relative to P^*. The corresponding states along the M branch are also stabilized by the protein but by a smaller amount. The effect of the static field is found to be large enough to compensate for the intrinsic cost of charge separation in a low dielectric environment. Recent calculations of the electrostatic potential in RCs have alternatively used Coulomb's law to describe electrostatic effects[37] or a model where the potential from ionizable groups is assumed to be small.[39,40,43] The first approach is likely to overestimate the effect of charged groups in the protein by ignoring the screening due to the water surrounding the protein. The second assumes that this screening is sufficient to greatly reduce the impact of these charges. The calculations presented here include the effects of ionizable groups while accounting explicitly for the effects of solvent screening.

Methods

Free Energy Calculations. The free energy of charge separation in the protein, $\Delta G_{\text{(electron transfer)}}$, is divided into three independently calculated terms. These terms can be identified with the free energies of first carrying out charge separation in vacuum ($\Delta G_{\text{(vacuum)}}$), then moving the charged cofactors into a medium with the dielectric constant of the protein ($\Delta G_{\text{(reaction field)}}$), then adding the effect of the charges and dipoles in the surrounding protein ($\Delta G_{\text{(static field)}}$). Thus

$$\Delta G_{\text{(electron transfer)}} = \Delta G_{\text{(vacuum)}} + \Delta G_{\text{(reaction field)}} + \Delta G_{\text{(static field)}} \quad (1)$$

$\Delta G_{\text{(vacuum)}}$ is the free energy of charge separation (for example going from P^* to $P^+H_L^-$) in the gas phase. It is obtained either from the gas phase, semiempirical, quantum mechanical, ZINDO calculations of Thompson and Zerner[30] or is estimated by a simple Coulombic model described below. $\Delta G_{\text{(vacuum)}}$ includes the difference of the intrinsic, vacuum electron affinity of the electron donor and acceptor as well as the Coulombic attraction between charges in the newly formed ion pair. The ZINDO calculations should also include the higher order corrections due to interactions between the electronic states in the closely associated donor and acceptor.

$\Delta G_{\text{(reaction field)}}$, which is also referred to as the self-energy, Born energy, or solvation energy, is the difference in free energy of transferring the cofactors in their initial and their final ionization states from vacuum to a medium with the dielectric constant of the protein (2 or 4 in this work). This accounts for the reduction in the free energy of the new charges due to the rearrangement of the surroundings.

$\Delta G_{\text{(static field)}}$ is the difference in free energy of interaction of the cofactors in their initial and their final ionization states with the static electrostatic field from the charged and polar groups

in the protein. The charges in the protein are screened both by the dielectric response of the surrounding solvent and by any dielectric response of the protein and membrane. $\Delta G_{(static\ field)}$ is obtained from

$$\Delta G_{(static\ field)} =$$
$$\sum V_j(\text{from charges on protein})(q_j(\text{charged cofactor}) -$$
$$q_j(\text{neutral cofactor})) \quad (2)$$

$$= \sum V_j(\text{static field})\Delta q_{j(cofactor)} \quad (2')$$

where $V_{j(static\ field)}$ is the value of the potential due to the static field from the charges in the rest of the protein at cofactor atom j and q_j is the charge on atom j. The sum runs over all atoms in the cofactor. The potential is an equilibrium property of the protein, present before the photon is absorbed. In practice it is sometimes more convenient to calculate $\Delta G_{(static\ field)}$ from

$$\Delta G_{(static\ field)} = \sum (V_j(\text{from charged cofactor}) -$$
$$V_j(\text{from neutral cofactor}))q_j(\text{protein}) \quad (3)$$

$$= \sum V_j(\text{from } \Delta q \text{ on cofactor})q_j(\text{protein}) \quad (3')$$

i.e., the product of the change in potential due to the change in charge on the cofactor and the partial charges on the protein. Here the sum runs over all atoms in the protein. Of course expressions 2 and 3 yield the same result. Equation 2 is more convenient for obtaining the final $\Delta G_{(static\ field)}$, and 3 for determining interactions with specific sites in the protein. Each procedure avoids the need to calculate the potential at atoms which are charged during the solution of the Poisson equation.

Coulomb's law is used to find V_i in eq 2 or 3, when the dielectric constant in and around the protein is assumed to be uniform. Here

$$V_j = \sum \{q_i/(\epsilon r_{ij})\} \quad (4)$$

where ϵ is the dielectric constant, q_i is the charge, and r_{ij} is the distance between the charged site and the site where the potential is determined. The sum either runs over all atoms in the protein (for eq 2) or all atoms in the cofactor (for eq 3). However, the assumption of uniform dielectric constant is inappropriate, since the low dielectric protein and membrane are surrounding by the water. The Poisson equation (5) provides V_i from a given charge distribution, ρ, under conditions of discontinuous ϵ:

$$\nabla \cdot \epsilon(r)\nabla \Phi(r) = -4\pi\rho(r) \quad (5)$$

Electrostatic potentials are obtained from finite difference solutions to the Poisson equation using the DelPhi program.[44−46] Most applications of classical electrostatics have entailed solutions of the Poisson−Boltzmann equation which adds a term to the Poisson equation which accounts for the ionic strength effects due to mobile ions in solution. However mobile ions are found to make essentially no contribution to calculated potentials in the interior of RCs and for this reason, results are reported here for the Poisson equation alone.

DelPhi first maps the molecular system onto a 65^3 lattice by defining charges and radii for all atoms. Charges are distributed to nearby grid points. The midgrid positions within the protein or membrane are assigned a low dielectric constant (2 or 4 in this work) while exterior points, or cavities with a diameter greater than 2.8 Å are given a dielectric constant of 80 representing water. When membrane is included, all internal cavities are assigned the dielectric constant of the protein. The

Poisson equation is solved numerically to provide potentials at each grid point.[44−46] Potentials at individual atoms are obtained by interpolation.

The largest errors in the precision of the finite difference method result from the grid-based representation of the molecular surface. These errors are overcome using a focusing procedure which improves the accuracy of the potentials.[45] In the initial calculation, the largest dimension of the macromolecule fills 40% of the grid and the potentials at the lattice points on the boundary of the grid are approximated analytically using Coulomb's law. Each succeeding focused calculation provides an increase in resolution in a particular region while excluding distal areas from the calculation. However, interactions with distant sites are implicitly accounted for through the boundary conditions used in the finer grid. Five focusing runs are used for the calculations on the *Rps. viridis* RCs (19 841 atoms, 137 Å maximum extent) giving a final scale of 3.0 grids/Å. The potentials for a given atom are collected at the finest grid spacing which has the whole residue containing the atom within the grid.

The reaction field free energies or self-energies for the isolated cofactors are obtained by multiplying the potential from the real charges on the cofactor atoms by the induced charges calculated from the divergence of the potential at the molecular surface, i.e., at the dielectric discontinuity. The accuracy of this calculation was improved by the positional rescaling of the induced charge.[47]

Molecular System. Calculations were carried out using the *Rps. viridis* RC structure 1PRC from the Brookhaven Data Bank.[5,48] All crystallographic water molecules were treated as part of the protein. Protons were placed on the heavy atom structure using the program PROTEUS (A. Joguine and M. R. Gunner City College of New York, unpublished). PROTEUS orients the positions of protons on waters and hydroxyls to minimize the electrostatic interaction free energy of the proton with residues within 4.5 Å of the hydroxyl or water oxygen. The hydroxyl and water protons are the only atoms with partial charges that either are not taken directly from the PDB file or do not have their positions completely determined by the heavy atoms in the structure. The influence of the membrane was estimated by including a cube $72 \times 72 \times 33$ Å of low dielectric material surrounding the protein (see Figure 1). The short (33 Å) transmembrane dimension is comparable to the detergent layer shown in the neutron diffraction picture of the RCs.[49] This extends 6 Å beyond the non-heme iron that lies between Q_A and Q_B and ends at the level of the two Mgs of P.

Calculations reported for the isolated cofactors include all six cofactors and the four histidines that are axial ligands to the bacteriochlorophylls. The phytyl tails of the bacteriochlorophylls and bacteriopheophytins are truncated at the ether link between the atoms O2A and C1. O2A is included in the calculations.

Calculations that include the total protein use the following atomic radii: C 1.8 Å, N 1.5 Å, O 1.6 Å, H 1.2 Å, S 1.9 Å, and 1.45 Å for Fe and Mg.[50] These will be referred to radii I. Calculation of the reaction field energy of the isolated cofactors use somewhat larger radii which have been parameterized to reproduce the transfer free energies of aromatic groups from vacuum to nonpolar solvents (Sitkoff and Honig, unpublished results). The values are C 1.99 Å, H 1.36 Å, and 2.00 Å for N, O, and Mg. These are refered to as radii II.

The CHARMM partial charge set is used for the protein.[51] The SO_4 molecules, LDAO (lauryl dimethylamine oxide), BOG (β-octylglucoside), and dihydroneurosporene in the PDB file were uncharged. TIP3P charges were used for the 201 waters

in the crystal structure. All histidines were assumed to be neutral. Each has a proton on ND1, with the exception of His L 168, which has the proton on NE2 so it can ligand the actyl group of P. A +2 charge is placed on the non-heme iron near the quinones. For all Asp, Glu, Arg, Lys, and heme propionic acids, C and N termini are assumed to be ionized with the exception of Glu L 104, the C subunit C-terminal and the H subunit N-terminal. The C-terminal sequence, Ala-Ala-Ala-Lys, on the C subunit is missing from the structure and was not replaced. The N terminal of the H subunit has a formyl cap and is therefore neutral. The net charge on the protein is −6.00. A number of residues are excluded from the calculations of the total potential for reasons provided below. The potential from each of the omitted residues at each of the cofactors is provided in Table 3.

Electrostatic Model. The basic model used for most analysis of protein by Poisson−Boltzmann calculations treats the protein as a low dielectric cavity containing charges located at atomic centers, embedded in a high dielectric medium. To test the sensitivity of the results to various approximations and parameters of the calculations, $\Delta G_{\text{(static field)}}$ and $\Delta G_{\text{(reaction field)}}$ will be presented with a number of values for different parameters.

The dielectric constant of the protein (ϵ_{prot}). Results are presented using dielectric constants of 2 and 4 for the protein and membrane (ϵ_{prot}). A dielectric constant of 2, the high-frequency dielectric constant, provides a good estimate for the effects of electronic polarizability.[52] This value should be appropriate to describe the $\Delta G_{\text{(reaction field)}}$ formed immediately after light absorption as well as the screening of the permanent charges in the protein that produce $\Delta G_{\text{(static field)}}$ by the electrons. Results using a dielectric constant of 4 for the protein and membrane are also presented. An ϵ_{prot} of 4 provides an estimate of the effects of nuclear relaxation in response to a change in the charge state of the system.[52] This reorganization will not contribute to the free energy of the initial charge separated states but it may provide a more realistic value of the $\Delta G_{\text{(electron transfer)}}$ for the equilibrated system. A value of 4 has been quite successful in describing equilibrium values for the charge transfers measured by electrochemical midpoints[53] and the pK_a's of ionizable groups in RCs[54−56] and other proteins.[57−60] In addition, a larger value of ϵ_{prot} may be needed for modeling the impact of mutations since changes in the protein will invoke compensatory rearrangements in the surrounding protein. Thus, the predicted effect of a mutation on the $\Delta G_{\text{(static field)}}$ would almost certainly be smaller than predicted with an ϵ_{prot} of 2.

Definition of Regions with Different Dielectric Constants. Three different models for the dielectric response of the system were tested. One uses a uniform dielectric constant of 2 (or 4) everywhere and is designated 2:2 (or 4:4) for ϵ_{prot}:ϵ_{solv}. The relevant potentials were determined directly from Coulomb's law. The protein embedded in a low dielectric slab, surrounded by water is designated 2:80:2 (or 4:80:4) for ϵ_{prot}:ϵ_{solv}:ϵ_{mem} (see Figure 1). The protein in water with no membrane, is designated 2:80 (or 4:80). Potentials for the protein in water, with or without the membrane, were obtained from solutions of the Poisson equation.

Charge Distribution on the Cofactors. Results are presented using two different charge distributions on the cofactors. In one, the ionized cofactors are represented with a charge of −0.25 on each N of B_L^-, B_M^-, H_L^-, or H_M^- or 0.125 on each N of P^+. Partial charges on the neutral cofactors and on P* are taken as zero. This parametrization is referred to as 4N. A more realistic parametrization which distributes charge over the entire macrocycle for both neutral and ionized cofactors is provided by the work of Parson et al.[43] Here, the charges for neutral or

TABLE 1: Electrostatic Potentials at the Cofactors[a]

dielectric constant	potential (mV)					
	2:2	2:80:2	2:80	4:4	4:80:4	4:80
P	−1171	−308	−387	−585	−168	−200
B_M	−1266	−393	−364	−633	−212	−194
B_L	−834	−42	−158	−417	−30	−84
H_M	−329	342	38	−165	163	28
H_L	−170	482	156	−85	241	88

[a] The potential due to CHARMM charges on all atoms in the protein, TIP3P charges on the water, and +2 on the non-heme iron, with dielectric constants given as ϵ_{prot}:$\epsilon_{solvent}$ or ϵ_{prot}:$\epsilon_{solvent}$:$\epsilon_{membrane}$. The position of the membrane is shown in Figure 1. Charges on the cofactors themselves and side chains of the residues in Table 3 are set to zero. The potential is averaged over the nitrogens at the center of each macrocycle.
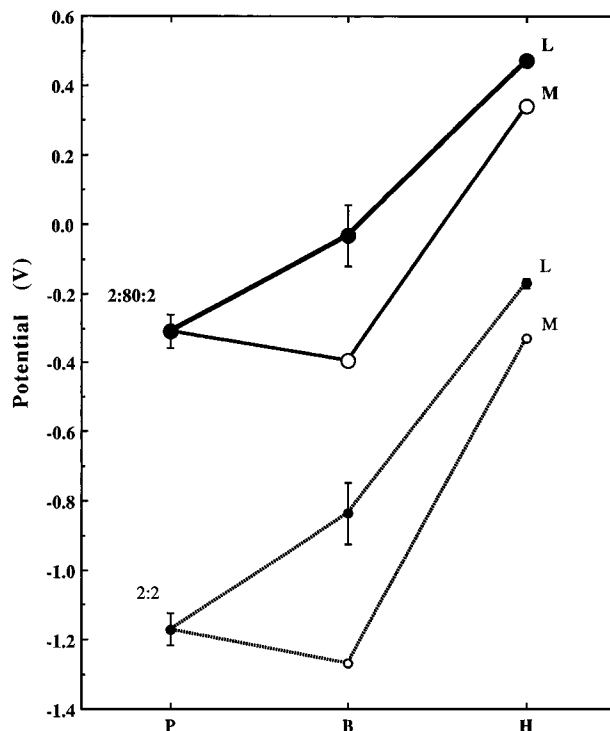
Figure 2. Potentials at the cofactors in the *Rps. viridis* RC from the charged and polar residues in the protein. Values are taken from Table 1. The error bar refers to two extreme positions of the hydroxyl proton on Tyr M 208 (see Table 3). The calculations labeled 2:2 are the potentials with a uniform dielectric constant of 2. The 2:80:2 calculations have the protein ($\epsilon_{prot} = 2$), embedded in a rectangular membrane ($\epsilon_{mem} = 2$), surrounded by water ($\epsilon_{solv} = 80$). (●) L branch cofactors; (○) M branch cofactors.

excited singlet P are those for two neutral BChls, while the charges for P^+ place half the charge of $BChl^+$ on each half of the dimer. This charge parameterization will be referred to as PCW.

Results

Potential at the cofactors due to the protein: Calculation of $\Delta G_{\text{(static field)}}$. Table 1 reports the potential (V) at the cofactors obtained with equation 3′ when water is included in the calculations or with eq 4 when the dielectric constant is uniform. The potential becomes increasingly more positive in going from P to B to H with all parameters tested. The difference in the potential (ΔV) favors forward electron transfer. In addition, the potentials on the L side of the protein are more positive than on the inactive M branch. Figure 2 shows that B_M is essentially isopotential with P, while B_L is in a region of the protein that is much more positive. Figure 3 shows the

Rhodopseudomonas viridis Reaction Centers

J. Phys. Chem., Vol. 100, No. 10, 1996 **4281**
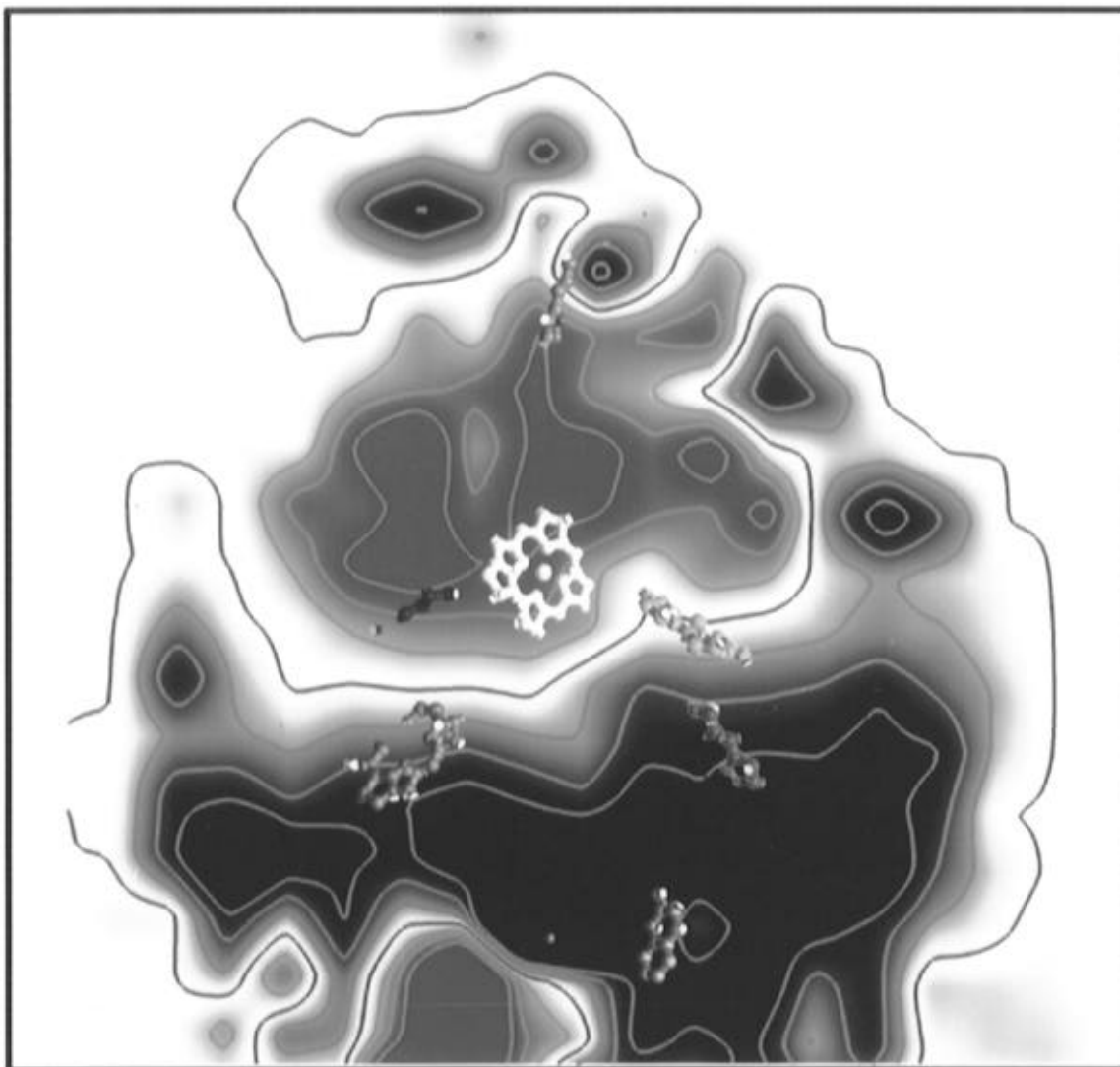
Figure 3. GRASP[110] representation of the potential through the RC prior to charge separation. The cofactors are P (white), B_L (yellow), H_L (green), B_M (dark blue), H_M (blue), Q_A, Fe^{2+}, and Q_B (silver). The slice plane cuts through the cofactors of interest. P_M and Q_A lie in front, while P_L and Q_B are behind the surface. The electrostatic potential was calculated under conditions 2:80:2. The slice plane surface and contours are coded so that blue is positive and red negative. The zero potential region of the slice plane is white. The isopotential contour at 0 V is green. The contours are at 0, ± 0.2, ± 0.4, and ± 0.6 V. The region below Q_B (bottom left) contains a cluster of acidic residues, which are expected to be only partially ionized in the RC ground state.[54,55] However, all the acids in the Q_B site were assumed to be ionized in the calculations presented here. This region of the protein is probably portrayed in this Figure as being too negative. Neutralizing the appropriate charges yields a small increase in $\Delta V_{(HM-P)}$.

potentials through a slice in the middle of the protein with neutral cofactors. This Figure graphically illustrates the negative potential near P and positive potential near H that will stabilize $P^+H_L^-$. In addition, the large potential gradient from P to B_L is clearly seen, while B_M is in a region where the potential is close to that found at P.

Both the value of the potentials at each site and the differences in potential between sites depend on the dielectric constants used in different regions. With a uniform dielectric constant of 2 the difference in potential at P and B_L ($\Delta V_{(BL-P)}$) is 337 mV and $\Delta V_{(HL-P)}$ is 1000 mV, implying there are very large fields within the protein. Even if a dielectric constant of 4 is used so the ΔVs are half as large, the static field is still significant. When screening of charges in the ground-state protein by water is taken into account, the potential at all the cofactors is much more positive than with a uniform dielectric constant (see Figure 2). The potential difference between sites is found to be less dependent on the dielectric model than the potential itself because the potentials at all sites exhibit a similar model dependence. However, the potential gradient along the reaction pathway in *Rps. viridis* does become smaller as the

protein is increasingly exposed to solvent. For example, $\Delta V_{(HL-P)}$ is 1000, 790, and 543 mV for dielectric assignments of 2:2, 2:80:2, and 2:80, respectively.

Table 2 reports the $\Delta G_{(static\ field)}$ obtained with eq 3′ for two distributions of the change in charge upon ionization of the cofactors. Despite the nonuniform potential through the RC, the calculated free energies are relatively insensitive to the exact cofactor charge distribution. The 4N and PCW charges yield differences of 35 meV or less for the effective potential at each site or the resultant $\Delta G_{(static\ field)}$. The text will focus on calculations with the PCW charges since they represent a more realistic picture of the change in charge distribution on the cofactors when they become ionized.

Sites That Are Not Included in the Calculated $\Delta G_{(static\ field)}$. The charges on Glu L 104, Tyr M 208, and the His side chains that provide axial ligands to the BChls (His L153, L173, M180, and M200) are set to zero. The contributions of these groups are listed in Table 3. Glu L 104 can hydrogen bond to the keto group of H_L when it is neutral. If it were charged, its close proximity to H_L would make forward electron transfer uphill. Site directed mutagenesis replacing this Glu with Leu

TABLE 2: Contribution of the Static Field of the Protein to the Free Energy of Charge Separation[a]

	$\Delta G_{\text{(static field)}}$ (meV)											
cofactor charges	4N			PCW			4N			PCW		
dielectric constant	2:2	2:80:2	2:80	2:2	2:80:2	2:80	4:4	4:80:4	4:80	4:4	4:80:4	4:80
P* → P$^+$B$_M^-$	95	85	−23	54	47	−47	48	44	−6	27	24	−24
P* → P$^+$B$_L^-$	−337	−266	−229	−374	−304	−259	−168	−138	−116	−187	−157	−136
P* → P$^+$H$_M^-$	−842	−650	−425	−837	−649	−432	−420	−331	−228	−418	−331	−234
P* → P$^+$H$_L^-$	−1001	−790	−543	−976	−767	−528	−500	−409	−288	−488	−398	−280

[a] $\Delta G_{\text{(static field)}}$ calculated with eq 2′. For the 4N charges Δq_i is zero for all atoms except the nitrogens at the center of the macrocycles; V_i's were taken from Table 1. The Δq_i for the PCW charges, which distribute the change in charge over the macrocycle, were taken from ref 43. The charge distribution on P* is either zero for the 4N charges or with the PCW charges each half of P has neutral BChl charges.

TABLE 3: Contributions to the Potential from Sites That Are Omitted from the Sums Given in Tables 1, 2, 5, and 6 (mV)

	2:2					2:80:2				
	P	B$_L$	B$_M$	H$_L$	H$_M$	P	B$_L$	B$_M$	H$_L$	H$_M$
	PCW Charges[a,b]									
His L 173	**−40**	−11	15	−4	2	**−40**	−11	15	−4	2
His M 200	**−39**	11	−12	1	−5	**−39**	10	−11	0	−5
His M 180	7	−3	**−68**	−2	−11	7	−3	**−69**	−2	−11
His L 153	−6	**−65**	−2	−2	−11	−7	**−67**	−2	−11	−2
sum	−78	−68	−67	−7	−25	−79	−71	−67	−17	−16
	4N Charges[b]									
His L 173	**−65**	−11	13	−4	2	**−65**	−10	12	−4	2
His M 200	**−55**	9	−11	1	−5	**−66**	8	−11	0	−5
His M 180	−7	−3	**−117**	−2	−11	−7	−3	**−118**	−2	−11
His L 153	−6	**−113**	−2	−2	−10	−7	**−115**	−2	−11	−2
sum	−133	−118	−117	−7	−24	−145	−120	−119	−17	−16
TyrM 208[c]	15	−81	9	5	8	16	−80	8	5	7
TyrM 208[d]	−48	91	−9	15	−3	−48	91	−9	15	−4
GluL104	−263	−336	−220	−790	−241	−87	−167	−57	−567	−72

[a] For PCW charges the potentials in the protein are a weighted average over the atoms that change charge on ionization. [b] The potentials due to the direct liganding histidine are in boldface. Tyr M 208 hydroxyl position that provides the (c) most positive potential or (d) most negative potential at B$_L$.

TABLE 4: $\Delta G_{\text{(reaction field)}}$ for the Cofactors Isolated from the Protein (eV)[a]

charge	4N	4N	4N	4N	PCW	PCW	PCW	PCW	PCW
ligands	no	yes	no	yes	no	yes	no	yes	yes
radii	I	I	II	II	I	I	II	II	II
dielectric constant	1:2	1:2	1:2	1:2	1:2	1:2	1:2	1:2	1:4
	A	B	C	D	E	F	G	H	I
P* → P$^+$B$_M^-$	−0.79	−0.61	−0.66	−0.50	−0.19	−0.39	−0.32	−0.38	0.61
P* → P$^+$B$_L^-$	−0.80	−0.60	−0.66	−0.49	−0.15	−0.35	−0.30	−0.35	0.56
P* → P$^+$H$_M^-$	−1.12	−1.03	−0.97	−0.90	−0.55	−0.70	−0.66	−0.69	1.12
P* → P$^+$H$_L^-$	−1.13	−1.04	−0.96	−0.90	−0.57	−0.70	−0.64	−0.68	1.09

[a] The atoms of all six cofactors are included in the low dielectric region for each calculation. Charge: The charge set used for the cofactor. The P* state uses the charge distribution of the ground-state P. With the PCW charges any uncharged cofactor has ground-state charges, which contribute significantly to the reaction field energy. $\Delta G_{\text{(reaction field)}}$ therefore has the reaction field energy of the P*B$_M$B$_L$H$_M$H$_L$ state of (A−D) 0 eV; (E) −1.68, (F) −0.95, (G) −0.91, (H) −0.54; (I) −0.94 eV subtracted from the reaction field energy of the charge separated states. Ligands: whether or not the four axial histidine ligands are included in the $\epsilon = 1$ region defined by the cofactors. Radii: radii I are smaller than radii II (see Methods). The dielectric constant is 1 inside the cofactors and 2 outside (A−H) or 4 outside (I).

or Gln in *Rb. capsulatus* RCs produces only small changes in the rates of formation of P$^+$H$_L^-$.[61]

The side chain of Tyr M 208 is also removed from the calculations of V and $\Delta G_{\text{(static field)}}$. This hydroxyl has a large impact on the potential, especially at B$_L$ (see Table 3 and Figure 2). However, there are no hydrogen bonds to this group, and when all the cofactors are neutral, the gradient of the electrostatic potential is insufficient to fix the hydroxyl proton position. In addition, this group has been removed from *Rb. sphaeroides* and *Rb. capsulatus* RCs with little change in rate or directionality of electron transfer.[62−67]

The contribution of the histidine ligands are included in the estimates of $\Delta G_{\text{(vacuum)}}$ (see below). Table 3 shows that if these His are treated explicitly, they have little effect on the electron transfer between P and either B since they lower the potential at all BChls by a similar amount. However, neither H has a

His ligand to lower its potential. Therefore, including a contribution of the electrostatic potential due to these ligands would increase the $\Delta V_{\text{(H−P)}}$ favoring charge separation.[43]

Estimates of the Intrinsic Cost of Charge Separation in Isolation from the Protein: Values for $\Delta G_{\text{(vacuum)}}$ and $\Delta G_{\text{(reaction field)}}$. *Free Energy of the Charge-Separated States in Vacuum.* The relative gas-phase energies of the electronic states of the cofactors in vacuum ($\Delta G_{\text{(vacuum)}}$), obtained from ZINDO calculations,[30] are shown in the third column of Table 5. The four His residues that are axial ligands to the bacteriochlorophylls were included in these calculations. Each of the four charge separated states were calculated to be approximately 1 eV higher in free energy than P*. The calculations thus predict that charge separation would not occur in vacuum. This result can be simply explained by noting that the modest differences in the intrinsic reduction potentials of a bacterio-

Rhodopseudomonas viridis Reaction Centers

J. Phys. Chem., Vol. 100, No. 10, 1996 **4283**

TABLE 5: Free Energy of Charge Separation[a]

	ΔÅ	contributors to the ΔG (meV)					resultant ΔG		
		ΔG_{v} 1:1	$\Delta G_{\text{r.f.}}$ 2:80:2	$\Delta G_{\text{s.f.}}$ 2:80:2	$\Delta G_{\text{r.f.}}$ 4:80:4	$\Delta G_{\text{s.f.}}$ 4:80:4	$\Delta G_{\text{(electron transfer)}}$		
							1:1	2:80:2	4:80:4
P* $\to$ P$^+$B$_{\text{M}}^-$	11.5	1080	-380	47	-612	24	1080	747	492
P* $\to$ P$^+$B$_{\text{L}}^-$	10.9	1040	-350	-305	-560	-158	1040	385	322
P* $\to$ P$^+$H$_{\text{M}}^-$	17.9	1130	-690	-650	-1117	-331	1130	-210	-318
P* $\to$ P$^+$H$_{\text{L}}^-$	17.8	1030	-680	-768	-1088	-398	1030	-418	-456

[a] ΔG_{v} is $\Delta G_{\text{(vacuum)}}$ is from ref 30. $\Delta G_{\text{r.f.}}$ is $\Delta G_{\text{(reaction field)}}$. Value for ϵ_{prot} of 2 is from column H and for ϵ_{prot} of 4 from column I of Table 4. $\Delta G_{\text{s.f.}}$ is $\Delta G_{\text{(static field)}}$ from Table 2. Resultant state free energies obtained from: $\Delta G_{\text{(electron transfer)}}(2:80:2) = \Delta G_{\text{vacuum}} + \Delta G_{\text{(reaction field)}}(1:2) + \Delta G_{\text{(static field)}}(2:80:2)$; $\Delta G_{\text{(electron transfer)}}(4:80:4) = \Delta G_{\text{vacuum}} + \Delta G_{\text{(reaction field)}}(1:4) + \Delta G_{\text{(static field)}}(4:80:4)$.

chlorophyll dimer, bacteriochlorophyll, and bacteriopheophytin which favor charge separation are smaller than the Coulomb attraction between unlike charges that favor charge recombination.

A rough estimate of the cost of charge separation in the gas phase can also be obtained from a simple model. Assuming that following light absorption to generate P*, an internal charge-transfer state is formed in P where a positive and negative charge are separated by 7.4 Å (the Mg−Mg distance). The Coulombic cost of moving an electron to B$_{\text{L}}$, where it is 10.9 Å from the center of the special pair, is 610 meV. Another 500 meV is then required to move the electron the additional 6.9 Å from B$_{\text{L}}$ to H$_{\text{L}}$. The 610 meV estimate of the cost of charge separation from P to B$_{\text{L}}$ would have to be added to the energy difference between P* and the internal charge-transfer state in order to obtain an estimate of the gas-phase energy difference between P* and P$^+$B$_{\text{L}}^-$. The excited-state energy levels in P are not well known, although P* is likely to be below the internal charge-transfer state. Thus, 610 meV represents the lower limit of $\Delta G_{\text{(vacuum)}}$ for the P* to P$^+$B$_{\text{L}}^-$ electron transfer.

In contrast to the P* to P$^+$B$_{\text{L}}^-$ electron-transfer process, the estimate of the Coulombic contribution to the cost of charge separation for the P$^+$B$_{\text{L}}^-$ to P$^+$H$_{\text{L}}^-$ transition in the gas phase is likely to be reasonably accurate since it does not depend on the relative placement of the excited state energy levels of P. It is then surprising, given the 500 meV cost of charge separation estimated above, that the semiempirical quantum mechanical calculations predict that P$^+$B$_{\text{L}}^-$ and P$^+$H$_{\text{L}}^-$ are essentially isoenergetic. One possibility that might account for the discrepancy is that the intrinsic differences in electron affinity between the BChl B and the BPh H are large enough to compensate for the cost of charge separation. However, BPh is only 230−250 meV easier to reduce than BChl in a variety of solvents. Moreover, there are only small changes when BChl aggregates are formed[68,69] suggesting that the difference in electron affinity is relatively insensitive to environmental effects.

An argument can be made that that experimental value of 250 meV in different solvents is also a good estimate for the gas-phase difference in electron affinity between the BChl B and the BPh H. BChl has an axial ligand while BPh lacks one in solution, in the vacuum calculations, and in RCs. The His ligand makes BChl harder to ionize because it reduces $\Delta G_{\text{(reaction field)}}$ (i.e., it removes solvent from the vicinity of the Mg^{2+}) and, in addition, imparts a negative potential at the macrocycle. Using PCW charges, and set II of atomic radii, the effect of the His ligand in different solvents has been calculated using a model where the internal dielectric constant, ϵ_{in}, of the macrocycle is assumed to be 2 while the "solvent" dielectric constant varies between 2 and 80. The calculated contribution of the His ligand to the relative electron affinity of BChl and BPh is 210 meV with ϵ_{out} of 10, 240 meV with ϵ_{out} of 80. In vacuum, the His contributes 280 meV. The insensitivity of these numbers to the exterior dielectric constant results from the fact that in

vacuum, the direct Coulombic interaction with the His which destabilizes the BChl$^-$ is largest since there is no solvent screening while, when ϵ_{out} increases, the Coulombic effect is reduced, but the reaction field stabilization of BPh$^-$ relative to BChl$^-$ increases. These calculations thus succeed in reproducing the measured electron affinity differences between BChl and BPh as well as their insensitivity to environmental factors. Moreover, they suggest that the measured value of 250 meV is also appropriate for the gas phase. Subtracting this value from the 500 meV Coulombic cost of charge separation leads to the prediction that P$^+$B$_{\text{L}}^-$ is 250 meV more stable than P$^+$H$_{\text{L}}^-$ in vacuum rather than being isoenergetic, as found in the ZINDO calculations. Nevertheless, the ZINDO values for $\Delta G_{\text{(vacuum)}}$ will be used for the remainder of the results section. The effect of the uncertainty in $\Delta G_{\text{(vacuum)}}$, especially on the relative energy of P$^+$B$_{\text{L}}^-$, will be considered in the discussion.

Contribution of the Reaction Field to the Free Energy of Charge Separation. $\Delta G_{\text{(reaction field)}}$ is the free energy to transfer the cofactors from the gas phase to a polarizable medium, assuming an interior dielectric constant of 1 for the cofactors. Values for $\Delta G_{\text{(reaction field)}}$ in going from the ground state to the different charge separated states are shown in Table 4. Results are reported for both the 4N and PCW charge distributions and for the two sets of atomic radii discussed above. With all parameters tested, $\Delta G_{\text{(reaction field)}}$ stabilizes the state with the largest distance between cation and anion. Thus, $\Delta G_{\text{(reaction field)}}$ tends to compensate for the reduction of favorable Coulomb interaction as the electron is moved further from P$^+$. $\Delta G_{\text{(reaction field)}}$ is quite sensitive to the charge distribution and also depends on the atomic radii and so will be a source of uncertainty in the final calculations. The values used in the final calculations use PCW charges and atomic radii based on organic solvent-transfer experiments (set II, Table 4 column H).

$G_{\text{(reaction field)}}$ was also calculated with ϵ_{in} of 1 and ϵ_{out} of 4 to provide an estimate of the reaction field energy in the protein after nuclear relaxation has occurred (Table 4 column I). The added stabilization provided by increasing the dielectric constant of the surroundings cannot be invoked to explain the initial stability of the charge separated states in RCs. These states are formed within 2 ps, even at 4 K, conditions where it is unlikely that the appropriate value for ϵ is much greater than 2.

Free Energy of Electron Transfer in Isolation from the Protein. The $\Delta G_{\text{(electron transfer)}}$ in a uniformly polarizable medium with no external charges is $\Delta G_{\text{(vacuum)}} + \Delta G_{\text{(reaction field)}}$ (Table 5). Using the ZINDO values for $\Delta G_{\text{(vacuum)}}$ of 1.03−1.13 eV for the four possible charge separated states, the change in reaction field energy must be at least this large for electron transfer to be favorable. Table 4 shows that $\Delta G_{\text{(reaction field)}}$ is generally not large enough to compensate for the gas-phase cost of charge separation. If the effective dielectric constant is assumed to be 2, the one exception is for the 4N charge distribution and smaller radii, but this is the least realistic parameter set.

There is little difference in $\Delta G_{\text{(reaction field)}}$ for charge separation to the L or M branch. A similar conclusion can be reached for $\Delta G_{\text{(vacuum)}}$ (see Table 5). Thus, the symmetry in the structure of L and M branches is mirrored in the free energies of the charge-separated states for the cofactors in isolation from the protein.

Driving Force for Electron Transfer in the Protein: Calculation of $\Delta G_{\text{(electron transfer)}}$. Values of $\Delta G_{\text{(electron transfer)}}$ for various electron-transfer processes are listed in Table 5. While the exact values are dependent on the parameters chosen, in all cases the intrinsic cost of charge separation in the gas phase is balanced by a potential gradient intrinsic to the protein and by the fast dielectric response due to electronic polarizability. For example, using a dielectric response of 2 for the protein and membrane and 80 for the surroundings, the 1030 meV cost of charge separation from P* to $P^+H_L^-$ in vacuum is compensated by a reaction field energy of -680 meV and a static field contribution of -768 meV to yield a reaction which is favored by -418 meV. Formation of $P^+H_M^-$ is also downhill but by 200 meV less. Reduction of either B is unfavorable, with B_M being 360 meV harder to reduce than B_L. As described above, the ZINDO values may overestimate $\Delta G_{\text{(vacuum)}}$ and thus $\Delta G_{\text{(electron transfer)}}$ from B to H by 250 meV. If the error is assumed to be in the energy of $P^+B_L^-$, then this state would lie 135 meV rather than 385 meV above P*. Alternately, the cost of forming $P^+H_L^-$ could be underestimated, placing this state 168 meV rather than 418 meV below P*.

Using a dielectric constant of 4 for the protein, the pattern for the relative free energies of the different charge-separated states is the same as with an ϵ_{prot} of 2. $P^+H_L^-$ is the lowest energy state, the reduction of H_M is favorable, and the reduction of neither B is energetically allowed. Changing ϵ_{prot} from 2 to 4 has only a minor effect on the calculated value of $\Delta G_{\text{(electron transfer)}}$ along the L branch, because as ϵ_{prot} increases the contribution of $\Delta G_{\text{(static field)}}$ decreases while that of $\Delta G_{\text{(reaction field)}}$ increases. The calculated asymmetry of the RCs is larger with the smaller ϵ_{prot} since $\Delta G_{\text{(static field)}}$ is the source of the difference between the L and M branches.

Sites in the Protein That Contribute to the Static Field Favoring Charge Separation. Figure 4 and Table 6 show the effect of the charged residues, polar side chains, backbone, and crystallographic waters on the potential. Ignoring the charged side chains and crystallographic waters, the potential from the protein is only 13 mV more positive at H_L than at P (see Figure 5). The potential from the charged groups is 642 meV more positive at H_L than at P, assuming all ionizable groups except Glu L 104 are charged. The crystallographic waters contribute 127 meV to make H_L more positive than P in the PROTEUS minimized structure. A large number of sites add to the potential gradient. The 45 side chains and 3 waters that contribute more than 25 mV to $\Delta V_{\text{(HL−P)}}$ are listed in Table 7.

Figure 6 illustrates the residues which provide more than 25 mV of the $\Delta V_{\text{(HL−P)}}$. The contribution to the potential at P is shown on the X axis with acids at negative and bases at positive values. Dipolar groups either raise or lower the potential. The difference in potential at P and H_L is plotted along the Y axis. Positive Y values favor electron transfer, since $V_{\text{(HL)}}$ is more positive than $V_{\text{(P)}}$, while negative values stabilize the electron on P. Thus, acids in the top left quadrant are on the periplasmic side of the protein, closer to P than H_L, and favor electron transfer. Bases in the bottom right quadrant are also closer to P than H_L and so oppose electron transfer. The favorable $\Delta V_{\text{(HL−P)}}$ can be seen immediately from a comparison of the top and bottom of the plot. The top half has a larger number of sites and larger Y values for a significant number of sites.
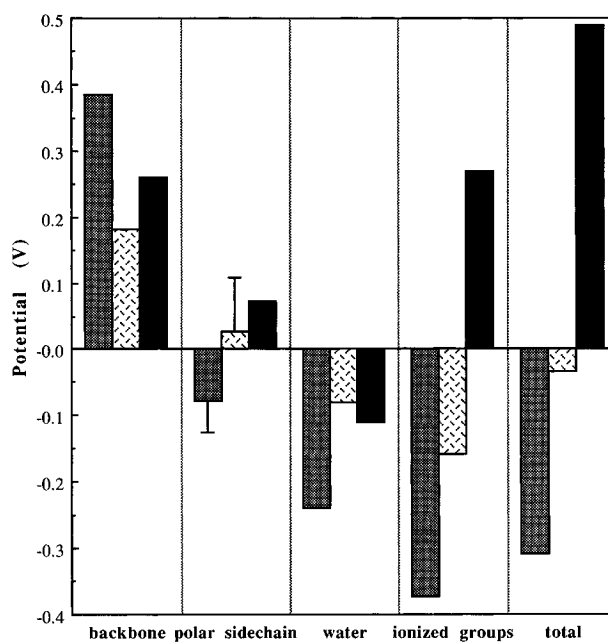
Figure 4. Contribution of different types of groups to the potential at P (grey), B_L (cross hatched), and H_L (black). Potentials taken from Table 6. The error bars on the contribution of the polar region show different possible contributions of Tyr M 208. Dielectric boundary conditions 2:80:2.

Arg L 103 and Fe^{2+} are the largest individual contributors to the potential gradient. The Fe^{2+} is bound within the protein by 4 histidines and a glutamic acid. Glu M 232, which ligands the Fe^{2+}, does oppose the effect of the iron as seen in Figure 6, but by a much smaller amount than the direct contribution of Fe^{2+}, both because it has a charge of $+1$ and because it is further from P and H_L than is the iron. Arg L 103 is is conserved in RCs from *Rps. viridis*, *Rb. sphaeroides*, and *Rb. capsulatus* as well as PSII.[70] The backbone of the protein is arranged to favor ionization of this base. Stabilization by the backbone rather than a counterion allows the charge to have maximal effect on $\Delta V_{\text{(HL−P)}}$ since the potential from the Arg^+ falls off much more slowly than the dipolar field of the oriented backbone dipoles. In addition, since the Arg is well buried its potential is not screened by solvent.

As has been noted previously, Asp H 36 and Arg H 33 are very close together and so their combined effect on $\Delta V_{\text{(HL−P)}}$ is small (-10 meV).[43] Asp M290 and Arg M 190 and Arg C 220 and Glu M 171 form two other ion pairs. None of the other ionizable side chains in Table 7 are in ion pairs.

The tables and Figures provide numbers calculated with the dielectric constants 2:80:2. Site interactions at 4:80:4 differ from simply half the 2:80:2 values by less than ± 10 meV. Again the difference between the interaction energies with 4N and CPW charged cofactors is less than ± 10 meV for any site except for the histidines which are the axial ligands to the BChls (see Table 3).

All other acids and bases in the protein make small contributions to $\Delta V_{\text{(HL−P)}}$. Preliminary calculations of site pK_a's (Gunner, unpublished) suggest that most buried residues are ionized. There is an extended cluster of 14 sites that are in close contact and include Glu H 177, Asp's H 236, M 2, and M 230, and Arg's H 181 and H 120 near the Q_B site which are most likely to be partially neutral.[54−56] These residues are found in the bottom left quadrant of Figure 6 and produce the negative potential region near Q_B in Figure 3. The predicted neutralization of some of these acidic residues would only serve to increase the potential gradient favoring electron transfer.

TABLE 6: Contribution of Different Types of Charges to the Potentials[a]

	potential (mV) (2:2)					potential (mV) (2:80:2)				
	bkbn	polar	wat	crg	sum	bkbn	polar	wat	crg	sum
P	944	−59	−248	−1807	−1170	383	−79	−239	−375	−309
B_M	739	−133	−88	−1784	−1266	146	−121	−71	−345	−392
B_L	738	57	−84	−1545	−835	181	26	−81	−159	−34
H_M	863	20	−65	−1147	−329	248	32	−48	107	340
H_L	921	58	−123	−1026	−170	260	57	−111	267	473

[a] Potentials are obtained as in Table 1. Bkbn is the amide dipoles of the protein backbone. Polar groups are the polar side chains. Crg represents the ionized side chains, chain termini, and nonheme Fe^{+2}. The charges on residues listed in Table 3 are set to zero.
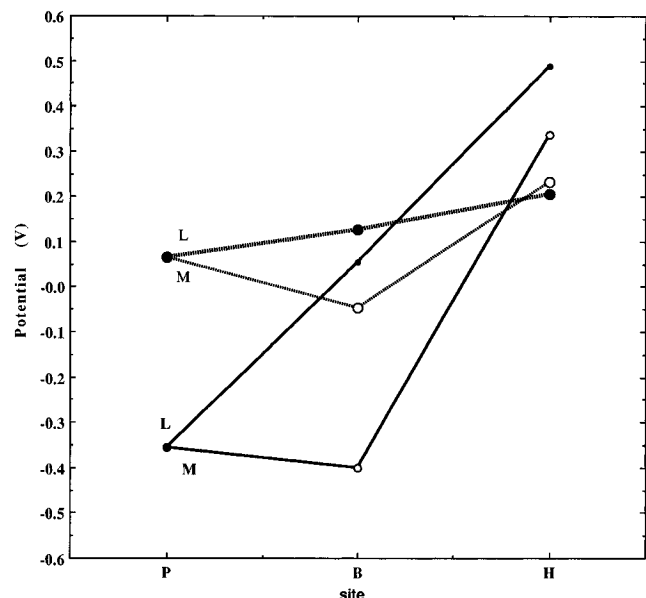
Figure 5. Comparison of the potential at the cofactors with (heavy line) and without (dashed line) charged side chains and Fe^{2+}. Dielectric boundary conditions 2:80:2. (●) L branch; (○) M branch.

The results of preliminary calculations on *Rb. sphaeroides* RCs also show a large $\Delta V_{(HL-P)}$. However, the cytochrome subunit that covers the periplasmic face of the *Rps viridis* but not *Rb. sphaeroides* RCs has significant impact on the contribution of specific sites to the static field. In particular, residues near P such as Asp L 155 and M 182 are buried by the C subunit in *Rps. viridis* RCs and so contribute to the field (see Figure 6). However, these residues have little impact in *Rb. sphaeroides* RCs since they are on the surface on the protein and are effectively screened by water.

Sites in the Protein That Contribute to the Difference in Potential along the L and M Branch of the Protein. A significant difference in the potential at B_L and B_M and a smaller difference between H_L and H_M is found for all parameters tested (see Table 1). Thus, the electrostatic potential strongly favors charge separation along the active branch of RCs (see Table 5). Although the magnitude of the $\Delta V_{(L-M)}$ is dependent on the dielectric constants used, the conclusion that the potential is asymmetric is independent of the parameters used in the calculations.

The potential along the L and M branches of the protein are compared in Tables 8 and 9 and Figures 7 and 8. Table 6 shows that the polar and charged sidechains are the most important contributors to $\Delta V_{B(L-M)}$ and therefore to $\Delta G_{(static field)}$. Table 8 shows the 22 ionized resides and two polar residues that contribute more than 25 meV to the difference. The sites that contribute to the asymmetry are widely distributed. In addition, over 100 meV of the total difference in the potential at the two BChls is contributed by sites which individually contribute less than 25 mV to $\Delta V_{B(L-M)}$.
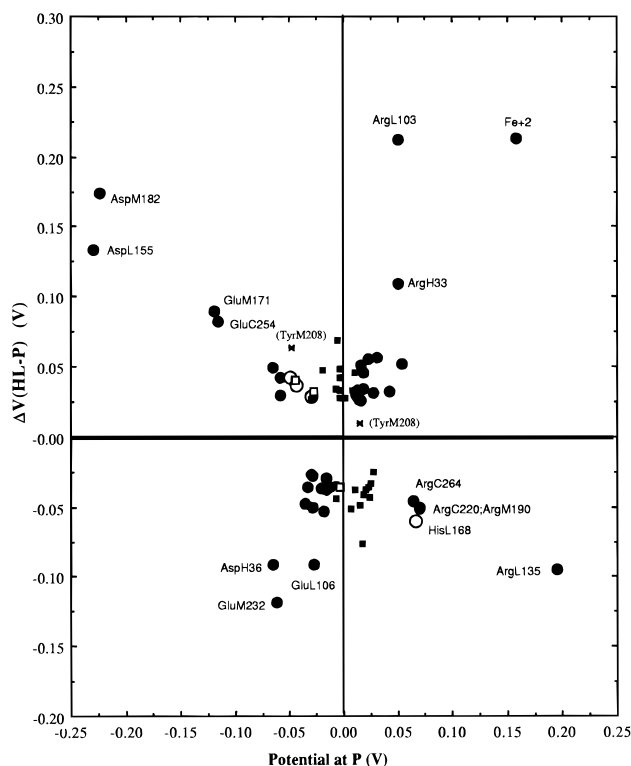
TABLE 7: Potential at the Sites That Contribute to the Difference in Potential at P and H_L by More Than 25 mV under Dielectric Boundary Conditions 2:80:2 (mV)

favor charge separation				oppose charge separation			
	P	H_L	dif		P	H_L	dif
Fe^{2+}	158	371	213	ASP H 36	−61	−180	−119
ARG L 103	50	262	212	ARG L 135	195	100	−95
ASP M 182	−224	−50	174	GLU L 106	−27	−119	−92
ASP L 155	−230	−97	133	GLU M 232	−66	−157	−91
ARG H 33	50	159	109	GLU L 6	−18	−71	−53
GLU M 171	−119	−29	90	ARG C 220	70	20	−51
GLU C 254	−115	−33	83	ARG M 190	70	19	−51
ARG H 37	31	87	56	ASP M 2	−29	−79	−50
ARG M 251	23	78	56	ASP M 230	−36	−83	−47
ARG L 231	54	105	52	ARG C 264	64	18	−46
LYS L 110	16	67	51	GLU H 39	−21	−57	−37
PRA[a]	−65	−16	49	GLU M 244	−16	−54	−37
ARG M 245	18	64	46	ASP L 23	−12	−48	−36
ASP M 290	−59	−17	42	GLU M 261	−34	−70	−36
ARG M 226	18	51	34	ASP H 236	−16	−46	−30
ARG L 10	13	46	33	GLU H 35	−29	−57	−28
ARG M 265	43	74	32	GLU H 177	−30	−57	−27
ARG H 181	27	58	31				
ASP H 11	−58	−28	30				
ARG L 109	12	41	29				
ARG M 239	13	40	27				
ARG H 120	16	42	26				
ASN M 193	−49	−7	42	HIS L 168	66	6	−60
ASN L 166	−44	−7	37				
ASN L 158	−29	0	29				
HOH 302	−27	5	32	HOH 305	−4	−39	−36
HOH 304	−45	−5	40				

[a] Pra is the propionic acid on the A ring of the heme closets to P.

Figure 7 shows the sites that contribute more than 25 meV to $\Delta V_{B(L-M)}$. In this plot, the residues that favor reduction of B_L are above the diagonal. These are either acids closer to B_M (bottom right) or bases closer to B_L. Symmetry-related sites such as Asp M 182 and L 155 or Arg L 103 and M 130 are found at comparable distances above and below the diagonal. Perhaps more interesting are sites which provide compensating interactions at the two BChls while not being at homologous positions on the L and M subunits. Examples include Glu M 171, M 76, and Asp L 218, which all lower the potential at B_M, and Asp H 36, L 60, and Glu L 106, which lower the potential at B_L. In addition, the contributions of Tyr M 208 in two different orientations is shown. The error bar in Figure 2, which represents the two extreme contributions of Tyr M 208 at B_L, shows that this residue has a large impact on the actual value of $\Delta V_{B(L-M)}$ but is not necessary for $\Delta G_{(static field)}$ to favor the L branch. The other hydroxy-containing side chains, Ser L 178 and L 152 which contribute significantly to the $\Delta V_{B(L-M)}$ have hydroxyl protons that are well fixed by hydrogen bond acceptors within the protein.

Figure 8 and Table 9 provide information about the residues that contribute to $\Delta V_{H(L-M)}$. A larger number of groups contribute more than 25 meV to the difference in potential than is found for $\Delta V_{B(L-M)}$. However, the resultant $\Delta V_{H(L-M)}$ is only

Figure 6. Sites that contribute more than 25 mV to the difference in potential at P and H_L given dielectric boundary conditions 2:80:2. ΔV_{HL-P} is plotted against V_P. Residues at positive Y values favor electron transfer from P to H_L. (●) Charged groups; (○) polar side chains; (□) waters; (■) backbone. Two positions are shown for Tyr M 208 (*). Residues contributing more than 60 mV to ΔV_{HL-P} are identified.

TABLE 8: Potential at the Sites That Contribute to the Difference in Potential at B_M and B_L by More Than 25 mV under Dielectric Boundary Conditions 2:80:2 (mV)

site			B_M	B_L	dif	symmetry-related site on homologous subunit		
ASP	M	182	−304	−81	223	Asp	L	155
ARG	L	135	80	176	96	His	M	162
ARG	L	103	32	108	76	Arg	M	130
GLU	M	171	−119	−50	68	His	L	144
ARG	H	33	36	88	52			
GLU	M	76	−68	−16	52	Gly	L	56
ARG	C	15	12	48	36			
ARG	H	37	23	53	30			
LYS	C	259	22	51	29			
ASP	L	218	−47	−19	28	Trp	M	252
ARG	M	86	38	12	−26	del		
ARG	C	220	62	34	−28			
GLU	L	106	−18	−52	−35	Ser	M	133
ASP	H	36	−49	−96	−47			
ASP	L	60	−18	−74	−56	Asp	M	80
ARG	M	130	96	28	−67	Arg	L	130
ASP	L	155	−82	−284	−202	Asp	M	182
SER	L	152	−3	−31	−28	Pro	M	179
SER	L	178	−52	3	55	Gly	M	205
TYR	M	208	−9	88	97	Phr	L	181
HOH		108	−3	−29	−26			
HOH		302	−7	28	35			
HOH		304	18	−10	−28			

half that of $\Delta V_{B(L-M)}$. Thus, the major distinction between the L and M branches is at the BChls rather than the BPhs.

Discussion

ΔG **for Charge Separation To Form $P^+H_L^-$.** The calculations presented above yield values of $\Delta G_{(electron\ transfer)}$ for

TABLE 9: Potential at the Sites That Contribute to the Difference in Potential at H_M and H_L by More Than 25 mV under Dielectric Boundary Conditions 2:80:2 (mV)

site			H_M	H_L	dif	symmetry-related site on homologous subunit		
ARG	L	103	39	262	223	Arg	M	130
ARG	H	33	56	159	103			
ASP	L	218	−111	−27	85	Trp	M	252
ARG	L	135	46	100	55	His	M	162
ASP	M	182	−103	−50	54	Asp	L	155
ARG	M	251	25	78	53	Arg	L	217
ARG	H	37	35	87	52			
LYS	L	110	15	67	52	Ala	M	137
GLU	L	212	−130	−79	51	Ala	M	246
GLU	M	171	−67	−29	38	Ser	L	152
ARG	M	245	26	64	38	His	l	211
ASP	M	43	−85	−50	35			
ARG	L	10	13	46	33			
ARG	L	109	11	41	30	Arg	M	136
GLU	M	244	−25	−54	−29	Glu	L	210
ASP	M	2	−47	−79	−32			
ASP	L	23	−10	−48	−38			
ARG	M	28	52	14	−38			
ASP	L	155	−51	−97	−46	Asp	M	182
ARG	L	217	84	37	−47	Arg	M	251
GLU	L	6	−20	−71	−51			
ARG	M	134	84	18	−66	Ile	L	107
ASP	H	36	−83	−180	−97			
GLU	L	106	−21	−119	−98	Ser	M	133
ARG	M	130	228	35	−193	Arg	L	103
SER	M	271	−32	8	40	Ala	L	237
ASN	L	183	−1	−26	−25	Cys	M	210
SER	L	238	3	−23	−27	Leu	M	272
ASN	M	147	62	−7	−69	Ala	M	120
HOH		301	13	−15	−28			
HOH		305	−3	−39	−36			

electron transfer from P* to $P^+H_L^-$ of −418 and −456 with dielectric models 2:80:2 and 4:80:4, respectively (Table 5). There is a considerable body of experimental evidence regarding the relative free energies of P* and $P^+H_L^-$.[71-74] Although most measurements have been carried out on *Rb. sphaeroides* RCs, the results are similar in *Rps. viridis* RCs.[2] There is good evidence that formation of $P^+H_L^-$ is a complex process. While $P^+H_L^-$ is initially formed approximately 150 meV below P*, in 10 ns it appears to have relaxed 100 meV,[11,71,75] in microseconds the state is 100 meV lower in energy,[76] and in milliseconds $P^+H_L^-$ is approximately 340 meV below P*.[71,77] The molecular origin of this relaxation is not known. The calculated $\Delta G_{(electron\ transfer)}$ values of approximately −400 meV are close to the experimental values determined on the millisecond time scale but are lower by about 250 meV than the −150 meV value for the initial formation of $P^+H_L^-$. Since our calculations refer specifically to fast events, (ϵ_{prot} of 2 accounts only for electronic polarization) our results appear to yield a free energy difference between P^* and $P^+H_L^-$ which is too negative by about 250 meV. Given the uncertainties in the calculations, particularly in the gas-phase energy levels, we regard this level of agreement between theory and experiment to be satisfactory. Moreover, the fundamental conclusion, that a large static field due to ionizable groups compensates for the intrinsic of charge separation in a low dielectric medium, is a robust result that is independent of the detailed model assumed in the calculations.

Electron Transfer from P* to B_L and P* to H_L: Can P^*B_L Be an Intermediate? B_L lies between P and H_L in the RC structure. The importance of B_L for function is inferred from the half time for reduction of H_L of 2 ps, a value which is orders of magnitude greater than expected for electron transfer over 18 Å if there is no intermediate electron acceptor.[15,16]

Rhodopseudomonas viridis Reaction Centers

J. Phys. Chem., Vol. 100, No. 10, 1996 **4287**
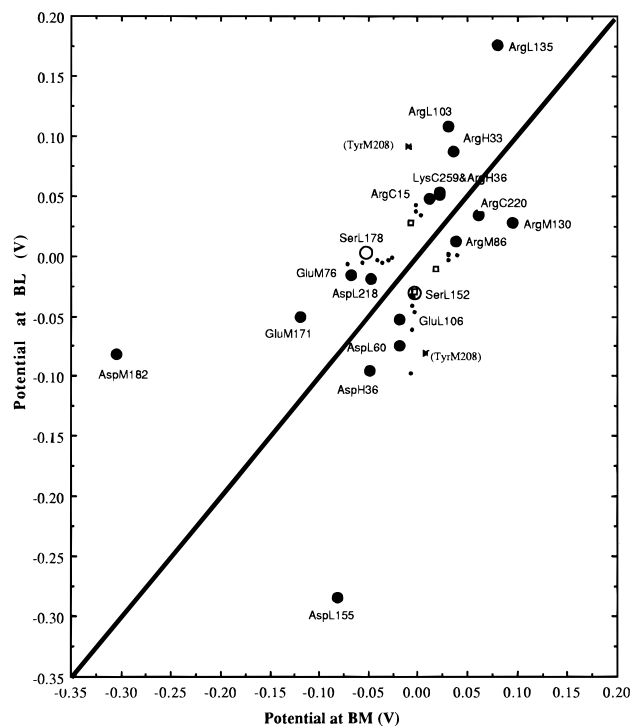
Figure 7. Sites that contribute more than 25 mV to the difference in potential at B_L and B_M given dielectric boundary conditions 2:80:2. The sites that favor electron transfer down the L branch are above the diagonal. (●) Charged groups; (○) polar side chains; (□) waters; (■) backbone. Two positions are shown for Tyr M 208 (*). Symmetry-related groups are often found equal distances above and below the diagonal.
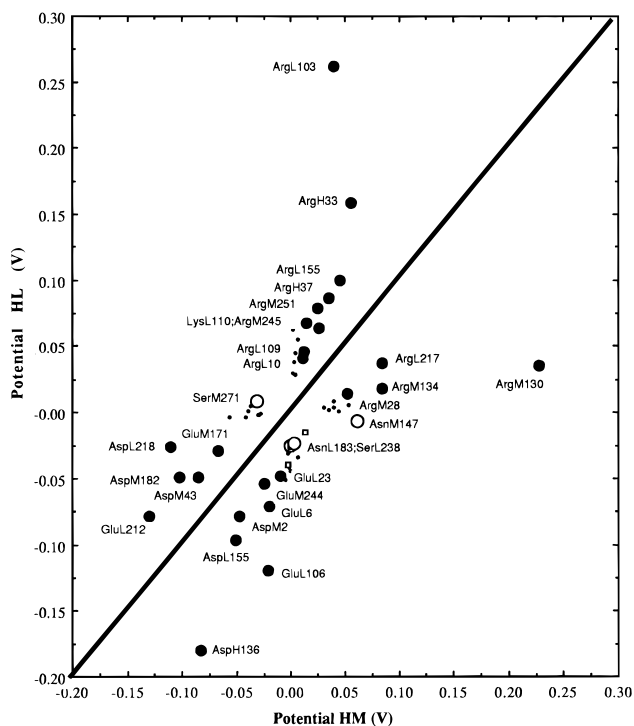
Figure 8. Sites that contribute more than 25 mV to the difference in potential at H_L and H_M given dielectric boundary conditions 2:80:2. The sites that favor electron transfer down the L branch are above the diagonal. (●) Charged groups; (○) polar side chains; (□) waters; (■) backbone. Symmetry-related groups are often found equal distances above and below the diagonal.

However, as has been described at length, B_L can facilitate electron transfer via a super-exchange mechanism and thus need not form a distinct, reduced intermediate.[17-24,78] With super

exchange the free energy of $P^+B_L^-$ could lie above P^*. However, if B_L is reduced in forward electron transfer, then it must lie near or below P^* to maintain the observed temperature independence of the forward electron-transfer rate.

Experimental evidence both supports and opposes mechanisms where B_L is reduced during charge separation.[22-24,79] Measurement of the time-resolved changes in the spectra of P, B, and H suggest that B_L is transiently reduced during charge separation to form $P^+H_L^-$.[22,80] Only a small amount is seen, consistent with $P^+B_L^-$ being formed more slowly than it decays. A mutant with a BChl at the H_L site, the "β" mutant, also suggests the free energy of $P^+B_L^-$ is below P^*. In this mutation, the 250 meV intrinsic difference in the reduction potential of BChl and BPh is removed. Spectroscopic evidence suggests that in this mutant the initial charge separated state has the electron delocalized over B_L, and β_L which is likely to require that $P^+B_L^-$ and $P^+\beta_L^-$ are close in energy and below P^*.[81,82]

Evidence opposing a linear, two-step model for electron transfer comes from the vibrational coherence of P^*, which decays with the rate at which $P^+H_L^-$ is formed.[83-85] In addition, the D_{LL} *Rb. capsulatus* mutant, which has no functional H_L,[86] shows no sign of transient reduction of B_L.[84] Also, a number of mutations have raised the free energy of P^+, reducing the gap between P^* and $P^+H_L^-$ with only limited effects on the electron transfer reaction.[87] Thus, while $P^+B_L^-$ may be transiently formed under some conditions, this may not be required for fast electron transfer.[23]

The calculations presented do not provide definitive answers as to the exact role of $P^+B_L^-$. The results shown in Table 5 place $P^+B_L^-$ about 380 meV above P^* which is too high for it to form a stable intermediate. However, this value depends strongly on the quantum mechanical calculations of $\Delta G_{(vacuum)}$ which, as discussed in the Results, may well be in error by a few hundred meV. Another way to approach this issue is to consider the relative free energy difference between $P^+B_L^-$ and $P^+H_L^-$. The results reported in Table 5 predict a value of about 800 meV, whereas if we correct the gas-phase energies by 250 meV as discussed in the Results, the free energy difference between these two states would be reduced to 550 meV. This would still place $P^+B_L^-$ about 100−400 meV above P^* with the exact value depending on the free energy difference assumed for P^* and $P^+H_L^-$. Two other sources of uncertainty are the reaction field energy (see Table 4) and the position of Tyr M 208 (see Table 3). If this Tyr hydroxyl is properly oriented, it could provide an additional 90 meV to stabilize $P^+B_L^-$.

Directionality of Electron Transfer in RCs. It is well established that electron transfer is predominantly along the L branch via H_L to Q_A. However, it is less clear what are the limits of the functional asymmetry. Monitoring charge separation at low temperature where the two BPhs are well resolved, shows that H_L is reduced, while there are no changes in H_M.[88] The resolution of these experiments places a limit on charge-transfer asymmetry of greater than 10 to 1. An additional demonstration of the unimportance of the M branch cofactors is that removal of H_M does not effect the rate or yield of formation of $P^+H_L^-$.[89] Under conditions where H_L is pre-reduced, P^* decays to the ground state before H_M is reduced by more than 9%, suggesting in normal RCs the electron transfer from P^* to H_L is at least 100 times faster than the rate of reduction of H_M.[90]

It is clear that there is a pronounced asymmetry in the electrostatic potential between the L and M branch cofactors. However, these calculations predict that $P^+H_M^-$ lies below P^* so that it would be stable if formed. In contrast, the formation of $P^+B_M^-$ is quite unfavorable. The high energy of this state

might then account for the inactivity of the M branch. Thus, the discrimination between the L and M branches appears to occur at the level of the BChls. The calculated value of $\Delta G_{B(L-M)}$ of -175 to -350 meV (for ϵ_{prot} of 4 and 2 respectively), while the $\Delta G_{H(L-M)}$ is only -70 to -120 meV. A large number of sites, often far from the cofactors, contribute to the asymmetry in the potential. The distribution of important residues may account for the difficulty of making mutants that favor electron transfer along the M branch.

Comparison of Results with Measurements on Modified RCs. Site-directed mutagenesis offers a direct means of testing the values for the impact of specific residues on the $\Delta G_{(static\ field)}$ listed in Tables 3 and 7−9. However, as described in the Methods, even small changes in protein structure would reduce the expected effect of the mutation. In the electrostatic formalism, this would appear as a larger effective ϵ_{prot} for the specific interaction with the mutated site. This is likely to be more important for mutations in charged sites than for polar sites. The effective dielectric constant will be assumed to be 4, which takes into account some molecular rearrangement on mutation of the protein. The calculated values for interaction energies with dielectric constants 4:80:4 are always very close to half of what is found with 2:80:2. Therefore, values in tables 3 and 7−9 will be divided by 2 in this section of the Discussion.

Many mutations have been made in RCs to explore the initial charge-separation event.[24,65,75,87,91−93] A surprising number have not stopped forward electron transfer even at low temperature. Most of the experiments have been carried out in *Rb. sphaeroides* RCs, with a number of mutations made in *Rb. capsulatus* RCs. The data base for *Rps. viridis* RCs is smaller. However, the behavior of all RCs is generally very similar.

Recently, a site-directed double, mutant in *Rb. capsulatus* RCs has been made that appears to show significant electron transfer to H_M.[94] One mutation substitutes His for Leu at L 212, resulting in BChl binding in the H_L site, producing the β_L phenotype. In addition, L 201 is changed from Gly to Asp. This Asp is close to B_L, apparently raising the free energy of $P^+B_L^-$. The mutant protein shows electron transfer to both β_L and H_M. If the new Asp is indeed ionized and does not perturb the structure too much, this result provides qualitative support for several conclusions of the calculations presented here. First, it indicates that electron transfer can occur down the M branch if electron transfer down the L branch is made unfavorable. Thus, the free energy of the charge-separated states controls the functional asymmetry, rather than unfavorable electronic coupling or protein reorganization energy on the M branch. Ionized side chains are capable of influencing these state energies, presumably through electrostatic interactions. In addition, it is a change at B_L that leads to electron transfer down the M branch. Thus, the directionality is controlled at the level of the BChls. Finally, since $P^+H_M^-$ is formed, its energy is indeed below that of P^*. Thus, these results are in agreement with the calculations presented here (see Table 5).

Tyr M 208 is conserved on the M branch of the three most studied bacterial RCs. It is not found in PSII RCs.[70] On the L branch this residue is replaced by a Phe. Earlier calculations,[43] suggested this residue could be important, and therefore it has been the focus of site directed mutants in *Rb. sphaeroides*[62−65] and *Rb. capsulatus* RCs.[66,67] P is found here to be 30 mV harder to oxidize when the Tyr is mutated to Phe in *Rb. sphaeroides* RCs, in good agreement with its calculated effect of 25 meV (ϵ_{prot} of 4) when it is in the orientation to provide the largest stabilization of B_L (see Table 3).

The non-heme iron between Q_A and Q_B appears to have a large effect on the $\Delta V_{(HL-P)}$. *Rb. sphaeroides* RCs can be prepared with no iron or other measurable divalent cation replacement.[95] While no measurements have been made of the cofactor midpoints in these RCs, there is little effect on the rate of formation of $P^+H_L^-$.[96] However it is reasonable to expect that uptake of protons into the Fe^{2+} site, perhaps on the histidines that ligand the iron, keeps $\Delta V_{(HL-P)}$ intact.

His L 168, which hydrogen bonds to the acetyl group of P_L, has been removed by site directed mutation in *Rb. sphaeroides* RCs, which lowers the midpoint of P by 80 mV.[91] This is larger than the 33 mV obtained here (ϵ_{prot} of 4) (see Table 7) Better agreement with experiment is obtained in this case if ϵ_{prot} of 2 is used, perhaps because the His is hydrogen bonded directly to the π system of P, or because the effects of nearby dipoles are best modeled with a lower dielectric constant.

The reduction of Q_A should provide a means to modify $\Delta V_{(HL-P)}$. An electron on Q_A lowers the potential at the nearby H_L more than P. The calculations predict that $\Delta V_{(HL-P)}$ should be reduced by 110 mV when Q_A is prereduced (ϵ_{prot} of 4). However, the free energy for charge separation, determined by the delayed fluorescence technique, changes by less than 40 meV.[11] One possible reason for the small measured change is that protons are bound from solution when Q_A^- is formed.[97,98] The uptake of positive charges, which will reduce the effect of the negative Q_A, is not taken into account in the calculations presented here. Also, protein relaxation in the presence of Q_A^- could screen the unfavorable interaction between H^- and Q_A^-. In contrast, measurements of the Stark shift at H_L due to Q_A^- do provide values for the effective dielectric constant for interactions between Q_A^- and H_L close to those calculated here. When RCs were prepared with Q_A^- at room temperature and then frozen, the effect of the new charge is significant, modeled with a ϵ_{eff} of 5.8.[99] The effect of the charge on Q_A^- at H_L, which is 13.5 Å away, is calculated to be 146 meV given dielectric constants 4:80:4. This is equivalent to an ϵ_{eff} of 7.2, in good agreement with the value extracted from the experiments.

Evidence for a Large Static Field within RCs. There have been many previous theoretical studies of electron transfer in RCs. However, none has explicitly discussed the difficulty of stabilizing charge separation in low dielectric material, especially at low temperature. The difficulty of forming stable, charge-separated states in low dielectric, nonpolar solvents is well known.[100−102] The particular difficulty of charge separation in frozen media due to the destabilization of the charge-separated state is demonstrated by the significant loss of driving force found for bridged donor−acceptor complexes upon freezing.[100,103] For example, in a porphyrin−triptycene accepter system with an 11 Å donor−acceptor separation, the charge separated state is 800 meV higher in energy in frozen 2-methyltetrahydrofuran ($\epsilon = 2.6$) than in liquid butyronitrile ($\epsilon = 20$) presumably due to loss of $\Delta G_{(reaction\ field)}$.[103] If these experiments with artificial donor−acceptor systems do model photosynthetic electron transfer, then charge separation would not occur between the RC cofactors at low temperature in isolation from the protein.

The presence of significant electrical fields within RCs from *Rb. sphaeroides* has been previously suggested by Middendorf et al.[104] based on Stark effect measurements. Their estimate for the matrix field at P is $>1.2 \times 10^6$ V/cm at 1.5 K. A $\Delta V_{(HL-P)}$ of 409 mV over the 17.8 Å distance between P and H_L implies an average field of 2.3×10^6 V/cm, which is consistent with their estimate.

Screening of Charges by Water and Protein. The correct value for the internal dielectric constant of a protein is uncertain. An ϵ_{prot} 2 appears to be formally correct since it accounts for

Rhodopseudomonas viridis Reaction Centers

J. Phys. Chem., Vol. 100, No. 10, 1996 **4289**

electronic polarizability, while the screening effects of protein dipoles are explicitly included in the partial charges that generate the static field and should thus not be included in the dielectric constant. However, prior calculations on redox potentials in *Rps. viridis* have provided a better match between theory and experiment with larger values for ϵ_{prot},[53] although these involved studies of themally relaxed states where a higher value of ϵ_{prot} is indeed appropriate. As described above, the use of ϵ_{prot} of 2 or 4 results in minor differences in the outcome of the calculations of the equilibrium ΔG for charge separation. Molecular dynamics calculations also provide evidence that there is some nuclear rearrangement that can occur rapidly following charge transfer that will increase the effective dielectric constant.[36–38]

The calculation of a large field through the protein rests upon the assumption that the protein screens charges to an extent represented by a dielectric constant of only 2–4, while the surrounding water has a dielectric constant of 80. The result is that charges on the surface have very little effect on the fields inside the protein, while charges buried within the protein can have a significant effect. It has been proposed that charges within the protein are generally stabilized by a counterion (e.g. a salt bridge), dipolar groups in the protein, or pockets of internal water molecules which reduce the effect of the charges.[105,106] In RCs the charges on a number of acidic and basic residues are found to be stabilized by dipolar groups in the protein. Arg L 103, which is a major contributor to the potential gradient, interacts with a region of the protein backbone which is oriented so as to provide a negative potential that is sufficient to compensate for most of the calculated loss in reaction field energy due to burial of the Arg. This dipolar field is strong at the nearby Arg but is negligible at the cofactors, while the monopole field from the Arg falls off much more slowly and so has a long range effect. In contrast, if a charge is stabilized by a counterion, a dipole is formed whose effects fall off more rapidly with distance. This is seen in the small net effect of the salt bridge Asp H 36, Arg H 33 on $\Delta V_{(HL-P)}$ (see Table 7).

Previous electrostatic calculations on *Rps. viridis* demonstrated that buried charged groups can have a significant effect on cofactor midpoint potentials. The equilibrium midpoints of the four hemes in the cytochrome subunit were obtained with the difference between the measured and calculated values of less than 60 meV.[53] The good match between experimental and calculated values is due in part to important contributions from the heme propionic acids and a buried Arg. In addition, the midpoint of the higher potential hemes is influenced by the potential from charges on the lower midpoint hemes which are ionized first in an equilibrium titration.

It is important to note that the reaction field of water induced by permanent charges and dipoles in the protein is present prior to light absorption. Therefore, it is appropriate to use the low-frequency dielectric constant of water (e.g., 80) to describe the screening of these charges even for electron-transfer events that are faster than the dielectric relaxation time of the solvent. That is, the solvent is polarized prior to light absorption establishing what is essentially a preexisting reaction field. Following light absorption, water molecules will reorient to "solvate" the newly formed charge distribution on a time scale that corresponds to the low frequency dielectric relaxation time. This effect is quite small for buried cofactors.

Much work on electron transfer in RCs has been carried out in frozen glasses. The potentials calculated here, which include screened charges, may also be appropriate for reactions at low temperature, if the water and protein retain their orientation as the protein is frozen. Measurements of the effect of charges

on the spectra in RCs show that solvation effects are retained when the system is frozen. If a charge is formed at 1.5 K, its effect at other sites in the protein is larger than when the charge is formed at room temperature and allowed to come to equilibrium before being frozen.[99] Since there can be only limited nuclear motion at 1.5 K the static field measured in the experiments of Steffen et al.[99] may be similar to that experienced by the electron at room temperature immediately following light absorption, where there is insufficient time for a nuclear response to electronic motion. The range of effective, low temperature, dielectric constants measured by Steffen et al. of 1.5–4.5 is consistent with the values used in this work.

Comparison with Earlier Calculations. Previous theoretical studies of the first steps in electron transfer in RCs have generally focused on the differential behavior of the L and M branches and the role of B_L. Explanations for the functional asymmetry include a different electronic coupling matrix element from P* to H_M and H_L,[25,27,32,107,108] differences in mobility and reorganization energy,[34–38,99] and differences in equilibrium driving force due to the difference in the electrostatic potentials on L and M branch.[41–43,109] Each of the earlier studies of the electrostatic potentials noted asymmetries in the potential at the L and M branch cofactors. In addition, a gradient of the potential between P and H comparable to what is found here was previously noted by Yeates et al.[41]

The calculations reported here suggest that a static electrostatic field, due primarily to charged amino acids in the protein, is largely responsible for directing electron transfer in RCs and is thus responsible for the observed asymmetry. This finding is based on an electrostatic model that makes no a priori assumptions about the charged state of individual residues or of the magnitude of the screening effect of the aqueous phase. Other effects, for example resulting from nuclear motion, may also contribute, but the static effects described here are so large that they would be expected to dominant the energetics of the electron transfers.

The molecular dynamics study of Marchi et al.[37,38] implicitly included both dynamic and static electrostatic effects and no attempt was made to separate the two types of contributions. On the other hand, ionizable residues were assumed to be charged and a uniform dielectric constant of 2 was used to describe electrostatic effects. Therefore, it is likely that a static field similar to the one obtained here with the 2:2 dielectric model made a major contribution in the calculations of Marchi et al. (see Figure 2). As has been previously noted,[40] the neglect of $\Delta G_{(reaction\ field)}$ contributes to the very unfavorable position of $P^+B_L^-$ relative to P* in this work.

The recent studies of Parson, Warshel, and co-workers assume that charged groups are so heavily screened that they make little contribution to electron transfer.[39,40,43] As can be seen in Table 6, the calculations reported here would place $P^+H_L^-$ about 20 meV below P* using dielectric constants 4:80:4, even if the contributions of the ionized residues to the static field were ignored. This result is in the range reported by Warshel and colleagues, suggesting that the two sets of calculations are not inconsistent. In addition, Table 5 shows that the relative importance of $\Delta G_{(static\ field)}$ and $\Delta G_{(reaction\ field)}$ is very dependent on the value for ϵ_{prot}. However, an ϵ_{prot} of 4 is likely to be too large for fast processes and at low temperature and thus represents an overestimate of $\Delta G_{(reaction\ field)}$. Using an ϵ_{prot} of 2, charge separation is predicted here to be unfavorable in the absence of the static field. Thus, the fundamental difference between the two sets of studies is not in the theoretical approach but rather in the underlying physical assumptions about the dielectric response of proteins and the charge state of amino

acids. The importance of ionizable groups can be resolved experimentally, for example by studies of Arg L 103 mutants.

Conclusion

The fundamental question that has concerned theoretical and experimental studies of RCs in the period following the elucidation of the structure has been how the protein is designed to facilitate efficient electron transfer along the active pathway. We have partitioned this question into two parts. The first concerns the means of overcoming the intrinsic cost of charge separation in a low dielectric medium while the second concerns the preference for the L over the M branch. The results of this study suggest that the protein solves both problems through the creation of a large static electric field which is produced by the specific position of many charged groups within the protein.

References and Notes

(1) Feher, G.; Allen, J. P.; Okamura, M. Y.; Rees, D. C. *Nature* **1989**, *339*, 111.
(2) Gunner, M. R. *Curr. Top. Bioenergetics* **1991**, *16*, 319.
(3) Deisenhofer, J.; Norris, J. R. *The Photosynthetic Reaction Center*; Academic Press: San Diego, 1993; Vol. I, II.
(4) Deisenhofer, J.; Epp, O.; Miki, R.; Michel, H. *Nature* **1985**, *318*, 618.
(5) Deisenhofer, J.; Michel, H. *EMBO J.* **1989**, *8*, 2149.
(6) Lancaster, C. R. D.; Ermler, U.; Michel, H. In *Anoxygenic Photosynthetic Bacteria*; Blankenship, R. E., Madigan, M. T., Bauer, C. E., Ed.; Kluwer: Dordrecht, 1995; p 503.
(7) Allen, J. P.; Feher, G.; Yeates, T. O.; Komiya, H.; Rees, D. C. *Proc. Natl. Acad. Sci. U.S.A.* **1988**, *85*, 8487.
(8) El-Kabbani, O.; Chang, C.-H.; Tiede, D.; Norris, J.; Schiffer, M. *Biochemistry* **1990**, *30*, 5361.
(9) Chang, C.-H.; El-Kabbani, O.; Tiede, D.; Norris, J.; Schiffer, M. *Biochemistry* **1990**, *30*, 5352.
(10) Ermler, U.; Fritzsch, G.; Buchanan, S. K.; Michel, H. *Structure* **1994**, *2*, 925.
(11) Woodbury, N. W. T.; Parson, W. W. *Biochim. Biophys. Acta* **1984**, *767*, 345.
(12) Horber, J. K. H.; Gobel, W.; Ogrodnik, A.; Michel-Beyerle, M. E.; Cogdell, R. J. *FEBS Lett.* **1986**, *165*, 107.
(13) Horber, J. K. H.; Gobel, W.; Ogrodnik, A.; Michel-Beyerle, M. E.; Cogdell, R. J. *FEBS Lett.* **1986**, *198*, 273.
(14) Marcus, R. A.; Sutin, N. *Biochim. Biophys. Acta* **1985**, *811*, 265.
(15) Moser, C. C.; Keske, J. M.; Warncke, K.; Farid, R.; Dutton, P. L. *Nature* **1992**, *355*, 796.
(16) Moser, C. C.; Dutton, P. L. *Biochim. Biophys. Acta* **1992**, *1101*, 171.
(17) Marcus, R. A. *Chem. Phys. Lett.* **1987**, *133*, 471.
(18) Marcus, R. A. *Isr. J. Chem.* **1988**, *28*, 205.
(19) Holzapfel, W.; Finkele, U.; Kaiser, W.; Oesterhelt, D.; Scheer, H.; Stilz, H. U.; Zinth, W. *Chem. Phys. Lett.* **1989**, *160*, 1.
(20) Joseph, J. S.; Bruno, W.; Bialek, W. *J. Phys. Chem.* **1991**, *95*, 6242.
(21) Finkele, U.; Lauterwasser, C.; Struck, A.; Scheer, H.; Zinth, W. *Proc. Natl. Acad. Sci. U.S.A.* **1992**, *89*, 9514.
(22) Zinth, W.; Kaiser, W. In *The Photosynthetic Reaction Center*; Deisenhofer, J., Norris, J. R., Eds.; Academic Press: San Diego, 1993; Vol. II, p 71.
(23) DiMagno, T. J.; Norris, J. R. In *The Photosynthetic Reaction Center*; Deisenhofer, J., Norris, J. R., Eds.; Academic Press: San Diego, 1993; Vol. II, p 105.
(24) Kirmaier, C.; Holten, D. In *The Photosynthetic Reaction Center*; Deisenhofer, J. Norris, J. R., Eds.; Academic Press: San Diego, 1993; Vol. II, p 49.
(25) Warshel, A.; Parson, W. W. *J. Am. Chem. Soc.* **1987**, *109*, 6143.
(26) Parson, W. W.; Warshel, A. *J. Am. Chem. Soc.* **1987**, *109*, 6152.
(27) Scherer, P. O. J.; Fischer, S. F. *J. Phys. Chem.* **1989**, *93*, 1633.
(28) Scherer, P. O. J.; Fischer, S. F. *Chem. Phys. Lett.* **1992**, *190*, 574.
(29) Thompson, M. A.; Zerner, M. C.; Fajer, J. *J. Phys. Chem.* **1991**, *95*, 5693.
(30) Thompson, M. A.; Zerner, M. C. *J. Am. Chem. Soc.* **1991**, *113*, 8210.

(31) Creighton, S.; Hwang, J.-K.; Warshel, A.; Parson, W. W.; Norris, J. *Biochemistry* **1988**, *27*, 774.
(32) Warshel, A.; Creighton, S.; Parson, W. W. *J. Phys. Chem.* **1988**, *97*, 2696.
(33) Warshel, A.; Chu, Z. T.; Parson, W. W. *Science* **1989**, *246*, 112.
(34) Schulten, K.; Tesch, M. *Chem. Phys.* **1991**, *158*, 421.
(35) Nonella, M.; Schulten, K. *J. Phys. Chem.* **1991**, *95*, 2059.
(36) Treutlein, H.; Schulten, K.; Brunger, A. T.; Karplus, M.; Deisenhofer, J.; Michel, H. *Proc. Natl. Acad. Sci. U.S.A.* **1992**, *89*, 75.
(37) Marchi, M.; Gehlen, J. N.; Chandler, D.; Newton, M. *J. Am. Chem. Soc.* **1993**, *115*, 4178.
(38) Gehlen, J. N.; Marchi, M.; Chandler, D. *Science* **1994**, *263*, 499.
(39) Warshel, A.; Chu, Z. T.; Parson, W. W. *J. Photochem. Photobiol. A: Chem.* **1994**, *82*, 123.
(40) Alden, R. G.; Parson, W. W.; Chu, Z. T.; Warshel, A. *J. Am. Chem. Soc.,* submitted.
(41) Yeates, T. O.; Komiya, H.; Rees, D. C.; Allen, J. P.; Feher, G. *Proc. Natl. Acad. Sci. U.S.A.* **1987**, *84*, 6438.
(42) Zheng, C.; Davis, M. E.; McCammon, J. A. *Chem. Phys. Lett.* **1990**, *173*, 246.
(43) Parson, W. W.; Chu, Z.-T.; Warshel, A. *Biochim. Biophys. Acta* **1990**, *1017*, 251.
(44) Klapper, I.; Hagstrom, R.; Fine, R.; Sharp, K.; Honig, B. *Proteins* **1986**, *1*, 47.
(45) Gilson, M. K.; Honig, B. *Proteins* **1988**, *3*, 32.
(46) Nicholls, A.; Honig, B. *J. Comput. Chem.* **1991**, *12*, 435.
(47) Bharadwaj, R.; Windemuth, A.; Sridharan, S.; Honig, B.; Nicholls, A. *J. Comput Chem.* **1995**, *16*, 898.
(48) Bernstein, F. C.; Koetzle, T. F.; Williams, G. J. B.; Meyer, E. F.; Brice, M. D.; Rodgers, J. R.; Kennard, O.; Shimanouchi, T. F.; Tasumi, M. *J. Mol. Biol.* **1977**, *112*, 535.
(49) Roth, M.; Lewit-Bentley, A.; Michel, H.; Deisenhofer, J.; Huber, R.; Oesterhelt, D. *Nature* **1989**, *340*, 659.
(50) Gilson, M. K.; Honig, B. H. *Nature* **1987**, *330*, 84.
(51) Brooks, B. R.; Bruccoleri, R. E.; Olafson, B. D.; States, D. J.; Swaminathan, S.; Karplus, M. *J. Comput. Chem.* **1983**, *4*, 187.
(52) Honig, B.; Sharp, K.; Yang, A.-S. *J. Phys. Chem.* **1993**, *97*, 1101.
(53) Gunner, M. R.; Honig, B. *Proc. Natl. Acad. Sci. U.S.A.* **1991**, *88*, 9151.
(54) Gunner, M. R.; Honig, B. In *The Photosynthetic Bacterial Reaction Center: Structure, Spectroscopy and Dynamics II*; Breton, J., and Vermeglio, A., Eds.; Plenum: New York, 1993; p 403.
(55) Beroza, P.; Fredkin, D. R.; Okamura, M. Y.; Feher, R. *Biophys. J.* **1995**, *68*, 2233.
(56) Lancaster, C. R. D.; Michel, H.; Honig, B.; Gunner, M. R. *Biophys. J.*, submitted.
(57) Bashford, D.; Karplus, M. *Biochemistry* **1990**, *29*, 10219.
(58) Beroza, P.; Fredkin, D. R.; Okamura, M. Y.; Feher, G. *Proc. Natl. Acad. Sci. U.S.A.* **1991**, *88*, 5804.
(59) Yang, A.-S.; Gunner, M. R.; Sampogna, R.; Sharp, K.; Honig, B. *Proteins* **1993**, *15*, 252.
(60) Sampogna, R. V.; Honig, B. *Biophys. J.* **1994**, *66*, 1341.
(61) Bylina, E.; Kirmaier, C.; McDowell, L.; Holten, D.; Youvan, D. C. *Nature* **1988**, *336*, 182.
(62) Nagarajan, V.; Parson, W. W.; Gaul, D.; Schenck, C. *Proc. Natl. Acad. Sci. U.S.A.* **1990**, *87*, 7888.
(63) Wachtveitl, J.; Farchaus, J. W.; Das, R.; Lutz, M.; Robert, B.; Mattioli, T. A. *Biochemistry* **1993**, *32*, 12875.
(64) Mattioli, T. A.; Gray, K. A.; Lutz, M.; Oesterhelt, D.; Robert, B. *Biochemistry* **1991**, *30*, 1715.
(65) Nagarajan, V.; Parson, W. W.; Davis, D.; Schenck, C. C. *Biochemistry* **1993**, *32*, 12324.
(66) Chan, C.-K.; Chen, L. X.-Q.; DiMagno, T. J.; Hanson, D. K.; Nance, S. L.; Schiffer, M.; Norris, J. R.; Fleming, G. R. *Chem. Phys. Lett.* **1991**, *176*, 366.
(67) Jia, Y.; DiMagno, T. J.; Chan, C.-K.; Wang, Z.; Du, M.; Hanson, D. K.; Schiffer, M.; Norris, J. R.; Fleming, G. R.; Popov, M. S. *J. Phys. Chem.* **1993**, *97*, 13180.
(68) Cotton, T. M.; Van Duyne, R. P. *J. Am. Chem. Soc.* **1979**, *101*, 7605.
(69) Watanabe, T.; Kobayashi, M. *Chlorophylls* **1991**, 287.
(70) Williams, J. C.; Steiner, L. A.; Feher, G. *Proteins* **1986**, *1*, 312.
(71) Woodbury, N. W. T.; Parson, W. W.; Gunner, M. R.; Prince, R. C.; Dutton, P. L. *Biochim. Biophys. Acta* **1986**, *851*, 6.
(72) Shopes, R. J.; Wraight, C. A. *Biochim. Biophys. Acta* **1987**, *893*, 409.
(73) Ogrodnik, A.; Volk, M.; Michel-Beyerle, M. E. *Biochim. Biophys. Acta* **1988**, *936*, 361.
(74) Boxer, S. G.; Goldstein, R. A.; Lockhart, D. J.; Middendorf, T. R.; Takiff, L. *J. Phys. Chem.* **1989**, *93*, 8280.
(75) Peloquin, J. M.; Williams, J. C.; Lin, X.; Alden, R. G.; Taguchi, A. K. W.; Allen, J. P.; Woodbury, N. W. *Biochemistry* **1994**, *33*, 8089.
(76) Goldstein, R. A.; Takiff, L.; Boxer, S. G. *Biochim. Biophys. Acta* **1988**, *934*, 253.

Rhodopseudomonas viridis Reaction Centers

J. Phys. Chem., Vol. 100, No. 10, 1996 **4291**

(77) Gunner, M. R.; Tiede, D. M.; Prince, R. C.; Dutton, P. L. In *Function of Quinones in Energy Conserving Systems*; Trumpower, B. L., Ed.; Academic Press: New York, 1982; p 265.

(78) Won, Y.; Friesner, R. A. *Biochim. Biophys. Acta* **1988**, *935*, 9.

(79) Kirmaier, C.; Holten, D. *Biochemistry* **1991**, *30*, 609.

(80) Holzapfel, W.; Finkele, U.; Kaiser, W.; Oesterhelt, D.; Scheer, H.; Stilz, H. U.; Zinth, W. *Proc. Natl. Acad. Sci. U.S.A.* **1990**, *87*, 5168.

(81) Kirmaier, C.; Laporte, L.; Schenck, C. C.; Holten, D. *J. Phys. Chem.* **1995**, *99*, 8903.

(82) Laporte, L.; Kirmaier, C.; Schenck, C. C.; Holten, D. *J. Phys. Chem.*, in press.

(83) Vos, M. H.; Lambry, J.-C.; Robles, S. J.; Youvan, D. C.; Breton, J.; Martin, J.-L. *Proc. Natl. Acad. Sci. U.S.A.* **1991**, *88*, 8885.

(84) Vos, M. H.; Lambry, J.-C.; Robles, S. J.; Youvan, D. C.; Breton, J.; Martin, J.-L. *Proc. Natl. Acad. Sci. U.S.A.* **1992**, *89*, 613.

(85) Vos, M. H.; Rappaport, F.; Lambry, J.-C.; Breton, J.; Martin, J.-L. *Nature* **1993**, *363*, 320.

(86) Robles, S. J.; Breton, J.; Youvan, D. C. *Science* **1990**, *248*, 1402.

(87) Lin, X.; Murchison, H. A.; Nagarajan, V.; Parson, W. W.; Allen, J. P.; Williams, J. C. *Proc. Natl. Acad. Sci. U.S.A.* **1994**, *91*, 10265.

(88) Kirmaier, C.; Holten, D. *Photosynth. Res.* **1987**, *13*, 225.

(89) Fleming, G. R.; Martin, J. L.; Breton, J. *Nature* **1988**, *333*, 190.

(90) Kellogg, E. C.; Kolaczkowski, S.; Wasielewski, M. R.; Tiede, D. M. *Photosynth. Res.* **1989**, *22*, 47.

(91) Murchison, H. A.; Alden, R. G.; Allen, J. P.; Peloquin, J. M.; Taguchi, A. K. W.; Woodbury, N. W.; Williams, J. C. *Biochemistry* **1993**, *32*, 3498.

(92) Woodbury, N. W.; Peloquin, J. M.; Alden, R. G.; Lin, X.; Lin, S.; Taguchi, A. K. W.; Williams, J. C.; Allen, J. P. *Biochemistry* **1994**, *33*, 8101.

(93) McDowell, L. M.; Gaul, D.; Kirmaier, C.; Holten, D.; Schenck, C. C. *Biochemistry* **1991**, *30*, 8315.

(94) Heller, B.; Holten, D.; Kirmaier, C. *Science* **1995**, *269*, 940.

(95) Debus, R. J.; Feher, G.; Okamura, M. Y. *Biochemistry* **1986**, *25*, 2276.

(96) Kirmaier, C.; Holten, D.; Debus, R. J.; Feher, G.; Okamura, M. Y. *Proc. Natl. Acad. Sci. U.S.A.* **1986**, *83*, 6407.

(97) Maroti, P.; Wraight, C. A. *Biochim. Biophys. Acta* **1988**, *934*, 314.

(98) McPherson, P. H.; Okamura, M. Y.; Feher, G. *Biochim. Biophys. Acta* **1988**, *934*, 348.

(99) Steffen, M. A.; Lao, K.; Boxer, S. G. *Science* **1994**, *264*, 810.

(100) Overfield, R. E.; Scherz, A.; Kaufmann, K. J.; Wasielewski, M. R. *J. Am. Chem. Soc.* **1983**, *105*, 5747.

(101) Antolovich, M.; Keyte, P. J.; Oliver, A. M.; Paddon-Row, M. N.; Kroon, J.; Verhoeven, J. W.; Jonker, S. A.; Warman, J. M. *J. Phys. Chem.* **1991**, *95*, 1933.

(102) Warman, J. M.; Smit, K. J.; deHaas, M. P.; Jonker, S. A.; Paddon-Row, M. N.; Oliver, A. M.; Kroon, J.; Overering, H.; Verhoeven, J. W. *J. Phys. Chem.* **1991**, *95*, 1979.

(103) Gaines, G. L.; O'Neil, M. P.; Svec, W. A.; Niemczyk, M. P.; Wasielewski, M. R. *J. Am. Chem. Soc.* **1990**, *113*, 719.

(104) Middendorf, T. R.; Mazzola, L. T.; Lao, K.; Steffen, M. A.; Boxer, S. G. *Biochim. Biophys. Acta* **1993**, *1143*, 223.

(105) Honig, B. H.; Hubble, W. L. *Proc. Natl. Acad. Sci. U.S.A.* **1984**, *81*, 5412.

(106) Warshel, A.; Russell, S. T. *Q. Rev. Biophys.* **1984**, *17*, 283.

(107) Plato, M.; Mobius, K.; Michel-Beyerle, M. E.; Bixon, M.; Jortner, J. *J. Am. Chem. Soc.* **1988**, *110*, 7279.

(108) Michel-Beyerle, M. E.; Plato, M.; Deisenhofer, J.; Michel, H.; Bixon, M.; Jortner, J. *Biochim. Biophys. Acta* **1988**, *932*, 52.

(109) Parson, W. W.; Warshel, A. In *The Photosynthetic Reaction Center*; Deisenhofer, J., Norris, J. R., Eds.; Academic Press: San Diego, 1993; Vol. II, p 23.

(110) Nicholls, A.; Sharp, K.; Honig, B. *Proteins* **1991**, *11*, 281.